1983

Degradation of fracture toughness in steels due to prior strain: a predictive model.

Sanford, Gregory Benson.

Monterey, California. Naval Postgraduate School

NAVAL POSTGRADUATE SCHOOL
Monterey, California

THESIS

DEGRADATION OF FRACTURE TOUGHNESS IN STEELS DUE TO PRIOR STRAIN: A PREDICTIVE MODEL

by

Gregory Benson Sanford

June 1983

Thesis Advisor: K. D. Challenger

UNCLASSIFIED

SECURITY CLASSIFICATION OF THIS PAGE (When Data Entered)

REPORT DOCUMENTATION PAGE		READ INSTRUCTIONS BEFORE COMPLETING FORM
1. REPORT NUMBER	2. GOVT ACCESSION NO.	3. RECIPIENT'S CATALOG NUMBER
4. TITLE (and Subtitle) Degradation of Fracture Toughness in Steels Due to Prior Strain: A Predictive Model		5. TYPE OF REPORT & PERIOD COVERED Master's Thesis June 1983 6. PERFORMING ORG. REPORT NUMBER
7. AUTHOR(s) Gregory Benson Sanford		8. CONTRACT OR GRANT NUMBER(s)
9. PERFORMING ORGANIZATION NAME AND ADDRESS Naval Postgraduate School Monterey, California 93940		10. PROGRAM ELEMENT, PROJECT, TASK AREA & WORK UNIT NUMBERS
11. CONTROLLING OFFICE NAME AND ADDRESS Naval Postgraduate School Monterey, Calfiornia 93940		12. REPORT DATE June 1983 13. NUMBER OF PAGES 82
14. MONITORING AGENCY NAME & ADDRESS(if different from Controlling Office)		15. SECURITY CLASS. (of this report) 15a. DECLASSIFICATION/DOWNGRADING SCHEDULE

16. DISTRIBUTION STATEMENT (of this Report)

Approved for public release, distribution unlimited.

17. DISTRIBUTION STATEMENT (of the abstract entered in Block 20, if different from Report)

18. SUPPLEMENTARY NOTES

19. KEY WORDS (Continue on reverse side if necessary and identify by block number)

Fracture Toughness
Plane Strain Fracture Strain
Crack Opening Displacement
Stretch Zone Width
HY-Series Steels
J-Integral
Microvoid Coalescence
Prestrain

20. ABSTRACT (Continue on reverse side if necessary and identify by block number)

This thesis quantifies the relationship between prior plastic strain, fracture toughness (J_{Ic}), plane strain fracture strain (ε_{fps}), and yield strength (σ_y) of HY-series steels at room temperature. Based upon initial J-integral test results of compact tensile specimens that showed a reduction in the fracture toughness with increasing amounts of prestrain, a correlation has been developed where J_{Ic} is directly proportional

DD FORM 1 JAN 73 1473 EDITION OF 1 NOV 65 IS OBSOLETE
S/N 0102-LF-014-6601

UNCLASSIFIED
SECURITY CLASSIFICATION OF THIS PAGE (When Data Entered)

20. ABSTRACT (cont'd)

to ε_{fps} to the fourth power. Thus, small changes in ε_{fps} will cause large changes in J_{Ic}. Further, it has been found that prestrain reduced ε_{fps} by an amount equal to the prestrain. The combination of these two correlations provides a very simple method of estimating the fracture toughness subsequent to plastic straining. Scanning electron microscopy was used to measure the crack tip stretch zone width (SZW), which is a good estimate of the crack tip strain prior to fracture. The SZW does decrease with increasing prior plastic strain verifying the decrease in ε_{fps}.

Degradation of Fracture Toughness in Steels Due to Prior Strain: A Predictive Model

by

Gregory Benson Sanford
Lieutenant Commander, United States Navy
B.S., University of Idaho, 1972

Submitted in partial fulfillment of the
requirements for the degree of

MASTER OF SCIENCE IN MECHANICAL ENGINEERING

from the

NAVAL POSTGRADUATE SCHOOL
June 1983

ABSTRACT

This thesis quantifies the relationship between prior plastic strain, fracture toughness (J_{Ic}), plane strain fracture strain (ε_{fps}), and yield strength (σ_y) of HY-series steels at room temperature. Based upon initial J-integral test results of compact tensile specimens that showed a reduction in the fracture toughness with increasing amounts of prestrain, a correlation has been developed where J_{Ic} is directly proportional to ε_{fps} to the fourth power. Thus, small changes in ε_{fps} will cause large changes in J_{Ic}. Further, it has been found that prestrain reduces ε_{fps} by an amount equal to the prestrain. The combination of these two correlations provides a very simple method of estimating the fracture toughness subsequent to plastic straining. Scanning electron microscopy was used to measure the crack tip stretch zone width (SZW), which is a good estimate of the crack tip strain prior to fracture. The SZW does decrease with increasing prior plastic strain verifying the decrease in ε_{fps}.

TABLE OF CONTENTS

LIST OF TABLES

LIST OF FIGURES

NOMENCLATURE

J	energy available for crack extension
J_{Ic}	critical value of J
K_{Ic}	critical plane strain fracture toughness value
T	tearing modulus
E	Young's modulus
SZW	stretch zone width
σ_y	yield strength
σ_f	flow stress
δ, COD	crack opening displacement
v	Poisson's ratio
ε_p	amount of prestrain
ε_{fps}	plane strain fracture strain
ε_{fps}	plane strain fracture strain at zero prestrain
$\varepsilon_{\theta_{ave}}$	average tangential strain
ε_y	longitudinal strain

ACKNOWLEDGMENT

I wish to express my sincere appreciation to my thesis advisor, Dr. Ken Challenger, for his patience and assistance with this work; and to Mr. Tom Kellogg for his invaluable assistance with all phases of my laboratory work. A debt of thanks is also given to my father for his continued encouragement and confidence in my academic endeavors. Lastly, I wish to especially thank my wife, Janice, for her constant support, understanding and love that sustained me in this effort and throughout my adult life.

I dedicate this work to Janice and my son, Lance.

I. INTRODUCTION

In 1981, David W. Taylor Naval Ship Research and Development Center (DTNSRDC), Annapolis, Maryland, began the project, "Ductile Fracture Characterization of Prestrained HY Steel Plate." A part of this project was to perform an analysis of the results obtained from the J-integral elastic-plastic fracture tests of prestrained and as-received HY steels and to complete a microfracture investigation of the compact tensile specimens used in the J-integral tests. The J-integral test results as reported by DTNSRDC indicated a reduction in the fracture toughness parameter J_{Ic} with increasing amounts of prestrain in HY-80, HY-100, and HY-130 steels. This thesis research has examined selected compact tensile specimens from all the HY-series steels tested. The fracture properties, the microstructure, and the effects of the alloying elements and their segregation on the reduction of J_{Ic} have been specifically examined and a quantifying relationship of their effect on the J_{Ic} degradation has been made. Scanning electron microscopy, optical microscopy, and electron microprobe analysis were used in this investigation.

The purpose of this work has been to identify the mechanisms responsible for the degradation of J_{Ic} in the HY-series steels with increasing amounts of prestrain, and to quantify the J_{Ic} degradation with respect to its non-prestrained material

parameters and the applied prestrain. Also, the J_{Ic} degradation with respect to its non-prestrained yield strength and variable stretch zone width is quantified.

The balance of this paper presents a background synopsis of the materials tested and the J-integral testing procedure used by DTNSRDC and their results, a brief outline of the laboratory techniques employed during this investigation, a discussion of the results obtained, and conclusions and recommendations.

II. BACKGROUND

A. HY STEELS

Since the mid 1950's usage of HY-80 steel has become wide spread in the Navy, with subsequent acceptance of the higher strengths HY-100 and HY-130 after their later development. These steels are the first high-strength quenched-and-tempered steels approved for use by the U.S. Navy for construction of large ocean vessels. They are low-carbon steels that achieve their strength and toughness through a quenching and tempering heat treatment. The chemical composition limits for these steels as required by military specifications are shown in Table I, {Ref. 1} and {Ref. 2}.

In these steels, a low carbon content was specified for good weldability. Close control of phosphorus and sulfur is required. The deleterious effect of sulfur results when it is combined with iron to form iron sulfide which is a liquid at normal rolling and forging temperatures. This tendency to hot-shortness can be successfully offset by the addition of manganese thus producing manganese sulfide instead of the harmful iron sulfide and limiting the sulfur content. Manganese is also added for solid solution strengthening. However, excessive amounts of manganese can cause embrittlement during heat treatment. Molybdenum is used to increase temper resistance by retarding softening during tempering of the

steel at high temperatures, to contribute significantly to hardenability, to improve creep resistance, and to improve machinability at high hardness levels. Nickel is primarily responsible for the good toughness, and the secondary effect of increasing hardenability. Chromium is added for hardenability and for its contribution to improved corrosion resistance. Silicon is used primarily as a deoxidizer {Ref. 3} and {Ref. 4}.

HY-80, HY-100, and HY-130 are fully killed, low alloy steels. The microstructures are predominantly martensitic for HY-130 and martensitic/bainitic for HY-80 and HY-100.

Procedures for the final quenching and tempering heat treatment used to obtain the required mechanical properties are left to the discretion of the steel producer. Military specifications impose only that the final minimum tempering temperature be 1100° F for HY-80, 1050°F for HY-100, and 1000°F for HY-130. Also, plates shall be water quenched after tempering {Ref. 1} and {Ref. 2}.

B. J-INTEGRAL TESTING

The J-integral is a mathematic expression, a line or surface integral that encloses the crack front from one crack surface to the other, used to characterize the local stress-strain field around the crack front. For elastic-plastic (linear and non-linear) solids for which the mathematical expression is path independent, the J-integral is equal to the value obtained from two identical bodies with infinitesimally

differing crack areas, each subject to stress, as the difference in loading work per unit difference in crack area at a fixed value of displacement, or when appropriate, at a fixed value of load {Ref. 5}.

The method employed by DTNSRDC involved digitizing analog load displacement data, and on-line, real-time computer interactive determination of crack length and J by an unloading compliance method. The immediate calculation of crack length allowed the test engineer to properly space unloadings, vary test machine speed, or vary unloading length during the test to obtain results from each specimen. Further, the method provided for storage of both digitized load displacement data and J versus crack extension data for future retrieval and analysis {Ref. 6}.

The test results reported herein utilized an Instron Model TTD universal test machine and a Tinius-Olsen test machine. The computer used for this testing was a Tektronix Model 4051. The detailed steps used to conduct the single-specimen J_{Ic} test can be found in {Ref. 6} and {Ref. 7}. J was then calculated according to the expression {Ref. 5},

$$J = \frac{A}{Bb} f\left(\frac{a_o}{w}\right) \left[1 - \left(\frac{.75f\left(\frac{a_o}{w}\right) - 1}{b}\right) \Delta a\right]$$

where:

A = area under load, load-point displacement record in energy units.

B = specimen thickness (for face grooved specimens B = B (net)).

w = specimen width

a_o = original crack size, including fatigue precrack

b = initial uncracked ligament, $(w-a_o)$.

$f\left(\frac{a_o}{w}\right)$ = a dimensionless coefficient value that corrects for the tensile component of loading. Values can be found in {Ref. 5}. Incrementing $f\left(\frac{a_o}{w}\right)$ for crack growth, Δa, is not necessary.

This equation includes a correction for crack growth.

J_{Ic} values were then computed from the intersection of the crack opening stretch line or blunting line ($J = 2\sigma_y \Delta a$) with the least squares fit of the data points which fell at least 51 microns beyond the crack opening stretch line and did not exceed approximately 1.5mm in crack growth. In this context σ_f is the average of the material yield strength and the ultimate strength and Δa is the crack extension {Ref. 7}.

The tearing moduli were calculated from an expression developed by Paris {Ref. 8},

$$T = \frac{E}{\sigma_o^2}\left(\frac{dJ}{da}\right)$$

where:

T = tearing modulus

J = slope of the J versus crack extension curve

E = elastic modulus, and

σ_o = flow stress

After testing, all specimens were heat tinted at 370°C for 30 minutes to mark the extent of crack growth.

Only those results from the DTNSRDC test that are applicable to this thesis are included in Tables II and III. The additional information will be contained in an as yet unpublished report by DTNSRDC Annapolis, Maryland.

III. EXPERIMENTAL

The twenty-one specimens examined in this work were all of the heat-tinted compact specimens used in the J-integral test conducted by DTNSRDC Annapolis, Maryland, which were made available to NPS. Each HY-series (80, 100, and 130) were represented by seven specimens. The composition and as-received measured strengths of the steels are listed in Table I. Two specimens of each alloy were tested in the as-received condition, while the other five specimens were tested at varying conditions of prestrain. Tables II and III identify the material, the prestrain condition, and DTNSRDC test results. All samples had been cut from the T-L orientation in the plate and those prestrained were prestrained in tension along the long transverse direction. Figure 1 depicts the orientation of the test specimens in the prestrained material.

The detailed description of the experimental investigation that follows was used on each of the twenty-one samples previously mentioned.

A new identification system using a single letter code was established to simplify data recording and material specimen marking. This coding system is defined in Tables II and III, with the original DTNSRDC specimen number shown for reference purposes.

To prepare the samples for Scanning Electron Microscope (SEM) and fractographic investigations, each had to be sectioned to meet equipment mounting limitations.

Before the sectioned fracture surface could be mounted for SEM observations, the oxidized layer (resulting from the heat tinting) had to be removed. This was accomplished by first applying acetone to both the fracture surface and one side of a piece of heavy cellulose acetate replicating tape (cut slightly larger than the specimen's surface area), and then mating the two. To insure an adequate bond, the tape was worked into the fracture surface using thumb pressure only so as to prevent damage to the specimen. After allowing the acetone to dry (approximately 10-15 minutes), the tape was carefully removed from the fracture surface. This procedure was repeated until no visible oxides or contaminants were removed with the replicating tape. Finally, the specimens were each ultrasonically cleaned in acetone for 15 minutes. This insured the removal of any tape traces embedded in the fracture surface.

At this point the clean fracture surfaces were mounted using Colloidal Silver on SEM pads and allowed to dry overnight for use in an S4-10 Stereoscan Scanning Electron Microscope (SEM).

SEM work included general observations of the fracture surface with corresponding photographs ranging from 20X to 1000X. More detailed attention was spent inspecting the stretch zone width (SZW) along the entire interface between the fatigue precrack region and the microvoid coalescence region. Representative photographs of the stretch zone for all specimens were taken at 200X and 500X magnifications.

Also, the stretch zone width was measured directly from the SEM CRT along the entire interface. An average stretch zone width for each specimen was calculated with Chauvenet's criterion {Ref. 9} applied for accuracy.

After completion of the scanning electron microscopy, several pieces of the original sample were sectioned for microstructural studies and to examine the material perpendicular to the fracture surface (both longitudinal and transverse); and specimens X, Y, and Z were prepared for direct review of the crack extension since these three specimens had not been stressed to final fracture. Each specimen was prepared for metallographic examination using standard procedures. Each sample was examined unetched and then etched lightly by swabbing the surface with a 2% nital solution. Observations of the microstructures were made on a ZEISS Universal Large Research Microscope. Lastly, one sample from each HY-series was specially prepared for an electron microprobe analysis using wavelength dispersive spectroscopy (WDS). The WDS was done by STRUCTURAL PROBE {Ref. 10} in Metuchen, New Jersey. Each sample was mounted in the phenolic mounts and polished as before, except that the final polishing was done using 1.0 and 0.5 micron Aluminum Oxide grit. Also, the mounts were cut so that the height of the mount was less than 8mm.

IV. RESULTS

A. J-INTEGRAL RESULTS

The results of the tests conducted by DTNSRDC indicate a reduction in the value of J_{Ic} with prestrain (see Table II). Figures 2, 3 and 4 depict graphically this relationship for the HY-80, HY-100, and HY-130 specimens respectively. In each case, the reduction from zero prestrain to five percent prestrain using the average values obtained for J_{Ic} was 23% for the HY-80 (interpolated from the maximum data provided), 29% for the HY-100 steel, and 32% for the HY-130 steel. Additionally, there was a reduction in the tearing modulus with increasing prestrain, as recorded in Table III. In DTNSRDC Report 81/027 (Ref. 11), the tearing instability using compact specimens is addressed in more detail.

It's important to note at this point that a relationship between J_{Ic} and prestrain exists; J_{Ic} decreases as prestrain increases. This important relationship will be further emphasized and re-enforced in the following chapters.

B. STRETCH ZONE WIDTH (SZW) RESULTS

The stretch zone widths for all specimens are listed in Table IV. Initial values for rough comparitive purposes where obtained by measuring the stretch zone width from representative SEM photographs for each specimen using the "average lines" technique. Figures 5, 6, and 7 show the

SEM photographs depicting the stretch zones (located between 1 and 2) for the three HY-series groups. Within each figure the obvious decrease of the SZW with increasing prestrain is evident. This measurement was in turn verified using the more accurate method of measuring the micrographs's stretch zone area using a K + E 4236 Compensating Polar Planimeter by Keuffel & Esser Co., and then computing the stretch zone width. Extremely good correlation between each pair of values was obtained. The final results presented in Table IV were obtained as discussed in the previous chapter by measuring the stretch zone width along the entire interface between the fatigue precrack and stable crack growth regions for each specimen from the scanning electron microscope screen. Again, the "average lines" technique was employed to obtain each screen measurement. Before averaging the measurements, the previously mentioned Chauvenet criterion was applied to improve the accuracy of the measurements taken, then the stretch zone width was calculated from the computed average. The SZW versus the amount of prestrain is shown in Figures 8, 9, and 10 for the HY-80, HY-100 and HY-130 specimens respectively.

C. MICROSTRUCTURAL INVESTIGATION

Micrographs of surfaces parallel to the fracture surface indicated the HY-80 and HY-100 specimens are primarily tempered martensite with a small percentage of bainite

{Ref. 12}. Inspection of the HY-130 specimens reveals a totally martensitic microstructure.

Obvious segregation/banding was visible under the light microscope and the results from an electron microprobe analysis performed by Mullican {Ref. 12} is presented. The analysis was made for Nickel (Ni), Iron (Fe), Chromium (Cr), Molybdenum (Mo), Vanadium (V), Silicon (Si), Sulfur (S), Carbon (C), and Manganese (Mn). Assuming a nominal variance of five percent, the following determinations were made. For the HY-80 specimens there was an increase in Ni, Cr, Mo, S, and Si in the dark regions; while Fe, Mn, V, and C showed no tendencies for preferential segregation. For the HY-100 samples there was an increase in Ni, Mn, Cr, Mo, S, and Si in the dark regions; while Fe showed no preferential tendency to segregate and V and C decreased in the dark regions. For the HY-130 specimens there was an increase in Mo, V, and S in the dark regions; while Ni, Fe, Mn, Cr, Si, and C all showed no tendencies for preferential segregation.

D. FRACTURE INVESTIGATION

Optical observation and low magnification examinations indicate that fibrous fracture occurred during the J-integral test. Examination of the fracture surfaces using the scanning electron microscope showed that increasing levels of prestrain produced more change in the topography of the HY-80 specimens, than the topography of the HY-100 and HY-130 specimens. In general, for all specimens, as the amount of prestrain was

increased the size and number of elongated troughs of apparently very low ductility, oriented in the rolled direction, also increased with some troughs at high prestrain levels in the HY-80 specimens demonstrating very narrow and deep trench-like formation. Figure 11 depicts the HY-80 normal trough formation compared to one of the high prestrain trench-like troughs extending well into the precrack region. Figures 12 and 13 show representative micrographs of the troughs for the HY-100 and HY-130 samples respectively as they transit through the stretch zone regions. Even though the number of these troughs increased with prestrain, they still represent only a small fraction of the overall fracture surface.

The overall fracture mode for the specimens was ductile rupture (microvoid coalescence) showing a dimpled fracture appearance, interspersed with large elongated troughs. The primary sites for initiation of the more equiaxed voids were probably carbides, separated in many areas by smaller voids nucleated at small carbide particles. The large elongated voids undoubtedly nucleated around a string of aligned inclusions where a low interface cohesive strength would be expected.

Also of major interest were two observations that seem contradictory to expected results. First, optical microscopy of the plane perpendicular to the fracture surface indicated that more microvoids were present below the fracture surface

for non-prestrained specimens than for the prestrained samples. Secondly, review of the crack tip region using the ZEISS microscope showed that for specimens with equal amount of prestrain, the HY-130 sample exhibited more microvoid formation than the HY-100 and HY-80 samples. In any case, no correlation between microvoid formation and elemental segregation (banding) was observed. Additionally, the microvoid size as determined from the SEM examination is very small and thus, only the largest microvoids would be seen with the optical microscope.

V. DISCUSSION

A. J_{Ic} DETERMINED FROM AMOUNT OF PRESTRAIN

The final equation expressing J_{Ic} in terms of plane strain fracture strain (ε_{fps}), which is dependent on the amount of prestrain, is very simplistic and extremely easy to work with. However, to fully appreciate its significance an in-depth review of its development is mandatory.

For any non-linear elastic body, J may be interpreted as the energy available for crack extension. The physical significance of J for elastic-plastic materials is that it is a measure of the characteristic crack tip elastic-plastic field. The J approach is normally limited to problems of plane strain or generalized plane stress. Another limitation is that unloading is not permitted if the deformation theory of plasticity is to be a realistic approximation of elastic-plastic behavior. Typically J-integral failure criterion is limited to the case of plane strain. As a consequence of the inadmissability of unloading and subcritical crack growth the critical value of J, J_{Ic} fracture criterion, refers to crack initiation rather than propagation {Ref. 13}.

For a valid plane strain fracture toughness test using J-integral criterion, the specimen thickness must be greater than a minimum value. Specifically {Ref. 14},

$$B \geq \alpha \left(\frac{J_{Ic}}{\sigma_y} \right)$$

where

B = specimen thickness

α = 38

ε_y = yield stress

This criterion was easily met by all the samples tested by DTNSRDC and examined in this work, as can be verified from the manufacturers' provided yield strengths in Table I and DTNSRDC J_{Ic} values in Table II.

In attempting to logically establish what mechanisms were active that were causing the reduction in J_{Ic} with increasing prestrain, an analytical approach was used.

J. F. Knott has shown that the critical J value, J_{Ic}, that occurs at crack initiation in plane strain is defined as follows {Ref. 15},

$$J_{Ic} = \frac{K_{Ic}^2}{E} (1 - v^2) \qquad (1)$$

where

K_{Ic} = critical stress intensity factor for plane strain mode I loading

v = Poisson's ratio

E = Young's Modulus

Also applicable for ferrous alloys ranging in strength from 80 ksi to 250 ksi is that {Ref. 4} and {Ref. 16},

$$K_{Ic} = A \sqrt{\sigma_y} (\varepsilon_{fps})^2 \quad (2)$$

where

A = constant for a given steel

σ_y = yield stress

ε_{fps} = plane strain fracture strain

Substituting equation (1) into equation (2) gives,

$$J_{Ic} = \frac{A^2}{E} (1-v^2) \sigma_y (\varepsilon_{fps})^4 \quad (3)$$

However, recognizing v and E as constants {Ref. 4}, the following equality is produced,

$$J_{Ic} = B\sigma_y (\varepsilon_{fps})^4 \quad (4)$$

where

B = constant for a given material

σ_y = yeild stress

ε_{fps} = plane strain fracture strain

At this juncture, it is important to define the terms in equation (4) as thoroughly as possible. ε_{fps} is specifically the plane strain fracture strain for the material after a specific amount of prestrain.

To make equation (4) a viable tool, a method for calculating ε_{fps} must be established. To compute ε_{fps} from the DTNSRDC results, a model developed by Bates and Santhanam, {Ref. 17}, for a smooth blunting notch under Type I loading is applied. They show that the average tangential strain around the crack tip surface is,

$$\varepsilon_{\theta_{ave}} = \ln \left[\left(1+ \frac{\delta}{2\rho}\right) * \left(1+ \frac{\delta}{\pi\rho\left(1+ \frac{\gamma}{\alpha}\right)}\right)^{-1} \right] \quad (5)$$

where

δ = crack opening displacement

ρ = initial crack tip radius

γ = crack extension due to blunting

α = the distance that the center of curvature of the notch recedes during blunting

Equation (5) assumes the notch has parallel flanks and a semicircular tip, and that $\frac{\gamma}{\alpha}$ approximates 0.2 {Ref. 17}.

Bates and Santhanam also proceed to show that the longitudinal strain (ε_y) at the notch tip is related to the average strain calculated above by,

$$\varepsilon_y = \varepsilon_{\theta_{ave}} \left(\frac{\pi}{2} - \frac{\omega}{2}\right)\cos\left(\frac{\omega}{2}\right) \quad (6)$$

where ω is the flank angle of the notch. In this case for a sharp crack, $\omega = 0$, thus equation (6) reduces to,

$$\varepsilon_y = \varepsilon_{\theta_{ave}} \left(\frac{\pi}{2}\right) \quad (7)$$

Recognizing that at fracture, $\varepsilon_y = \varepsilon_{fps}$ and $\delta = \delta_c$, and combining this knowledge with equations (5) and (7), the following valuable formula is obtained,

$$\varepsilon_{fps} = \frac{\pi}{2} \ln \left[\frac{1+ \frac{\delta}{2\rho}}{1+ \frac{\delta}{1.2\pi\rho}} \right] \quad (8)$$

The last hurdle in making equation (4) productive is to provide values for the initial crack tip radius, ρ, and the

critical crack opening displacement, δ_c, for insertion into equation (8). From experimental measurements, ρ was determined to be .001 inches for all samples tested. Next, Knott {Ref. 18} demonstrated the dependency of J on the crack opening displacement,

$$J = n\sigma_y\delta \tag{9}$$

where n is a geometrical factor, and σ_y is the previously defined yield strength without prestrain. Equation (9) can be further refined for the critical fracture point by accepting "n" equal to 1.8 based on the findings of De Castro et al {Ref. 19} and supported by Hertzberg {Ref. 4},

$$Jic = 1.8\sigma_y\delta_c \tag{10}$$

or re-written

$$\delta_c = \frac{J_{Ic}}{1.8\sigma_y} \tag{11}$$

Upon reaching this point, the values for J_{Ic} and σ_y for a given steel must be assembled. Table II provides J_{Ic} values for all specimens. Table VI is non-prestrained tensile test data for the HY-80 and HY-100 steel sample plates from DTNSRDC. Due to the absence of data for the HY-130 steel, the manufacturer's documented values from Table I will be used. With all this data assimilated, ε_{fps} can then be determined by applying sequencially equations (11) and (8). With these three values in hand, equation (4) can be implemented to determine the value B for that particular steel. For demonstration, these values are presented

in Table VII for the non-prestrained condition for each of the HY-series steels studied in this project.

The validity of equation (11) is re-enforced by the excellent comparison of this work's calculated critical crack opening displacement values and those found by Fields and Miller for HY-100 specimens {Ref. 20}. Specifically, Fields and Miller found for a range of 0% to 6% prestrain that the COD varied from 0.00669 inches to 0.00433 inches.

Next, Table VIII demonstrates the calculation of ε^{o}_{fps} exercising an assumption that,

$$\varepsilon_{fps} = \varepsilon^{o}_{fps} - \varepsilon_{p} \qquad (12)$$

where

ε^{o}_{fps} = plane strain fracture strain for zero prestrain

ε_{p} = specific amount of prestrain

The values shown have an average standard deviation of less than four percent, indicating that the assumption is very good. Concern at this point regarding the use of only the non-prestrained yield strength in the above equations can be alleviated by comparing Tables VIII and IX. Table VIII computes ε^{o}_{fps} for all specimens using the non-prestrained yield stress calculated in Table VII. Table IX, calculates ε^{o}_{fps} for the HY-80 and HY-100 specimens using the DTNSRDC data from Table VI and extrapolating as necessary the required prestrained values for yield stress. Recognizing that ε^{o}_{fps} should remain constant, comparison of the standard deviations examplifies the use of only the non-prestrained yield stress values, since they are more than twice as accurate.

Continuing, the J_{Ic} value for any steel can be computed for any given amount of prestrain by again applying equations (12) and (4), coupled with the established values for σ_y, ε^o_{fps}, and B in Table VII. This procedure is presented in tabular form for all the specimens in Table X, with the DTNSRDC experimentally determined J_{Ic} values conveniently listed for comparitive purposes.

Figures 14, 15, and 16 graphically display the excellent relationship of the plane strain fracture strain to the fourth power against the experimental J_{Ic} values reported by DTNSRDC for the HY-80, HY-100, and HY-130 steels respectively. These plots are further supported by the results of a linear fit to the data points of a log-log plot of J_{Ic} versus ε_{fps}. This plot had a slope equal to 3.989 which would represent the power factor of the ε_{fps} term. Figures 17, 18, and 19 follow with similarly fine plots of the calculated J_{Ic} values obtained using equation (4) as compared to the actual DTNSRDC J_{Ic} values. However, it should be pointed out that equation (4) tends to overpredict J_{Ic} values at low levels of prestrain. This indicates that something else is also a factor. In any case, though, the current established relationship gives a very good first estimate.

Equations (4) and (12) imply that small increases in the amount of prestrain, ε_p, will proportionally reduce the plane strain fracture strain, ε_{fps}, which will dramatically

affect the J_{Ic} value because of its dependence on ε_{fps} to the fourth power. The degradation of toughness is also critically dependent on both the direction of prestrain and the direction of loading. Equation (4) assumes like directions for both, which provides the most conservative estimate. Opposite loading directions of the two would yield higher J_{Ic} values {Ref. 21}.

The fracture surfaces without and with prestrain support the proposed reduction in ε_{fps}. Shallower dimples and an increasing number of large elongated troughs are observed on the fracture surfaces with increasing prestrain. It appears the prestrain led to easier microvoid nucleation, since the prestrained surfaces exhibited very limited plasticity which may have been caused by a decohesion of the interface between the matrix and the large inclusions associated with these elongated troughs.

The mechanism by which the prestraining has reduced the fracture ductility is not completely understood. Iricibar et al {Ref. 22} have shown that the strain required to nucleate a microvoid decreases linearly with the square of the hydrostatic component of stress. This would suggest that the strain required for nucleation of a microvoid would be path dependent and could be altered by not only prestrain, but also by the method of prestraining, i.e., tension versus compression. They have also shown that the strain required for void nucleation is dependent upon the particle size and location. Large particles located on

grain boundaries have a much lower void nucleation strain than do the smaller particles in the matrix. This also supports the explanation for the appearance of more low ductility troughs (large elongated microvoids) on the fracture surfaces of the materials with increasing prestrain.

Another possible explanation is that the prestraining may effect both processes of ductile fracture, void nucleation and void growth. The shallower microvoids (dimples) on the prestrained sample fracture surfaces suggest that the void growth behavior has been changed. The work of Tracey, {Ref. 23}, clearly shows that void growth is decreased by strain hardening. Thus, a complete understanding of how prestraining has altered the ductile fracture process requires an understanding of how the strain history has affected the strain hardening rate of the material.

With the information presently available it's impossible to separate the role of void nucleation from void growth, but the evidence strongly supports a damage mechanism where the summation of the two is reduced by prestrain.

The major cause for the reduced fracture toughness is believed to be a combination of residual stresses around carbide particles resulting from the prestrain, a reduction in void nucleation strain and a decrease in void growth resulting from changes in the local strain hardening behavior. But whatever the cause, the total strain at fracture has been reduced. In one case (void nucleation during prestraining),

the damage is permanent and non-recoverable; while if caused by residual stresses and reduced work hardening rates the damage could be completely recovered by stress relieving. Both Knott {Ref. 18} and Iricibar et al {Ref. 22}, have shown that stress relieving pre-strained steels at 950°F will restore the work hardening rate, will increase the strain at fracture and will restore the fracture toughness of the prestrained material to its original value.

It is postulated that the fracture toughness of the HY-series steels, subsequent to prestraining, could be restored by a stress relieving treatment. Further, it is believed that the reduction in toughness is due to a reduction in the plane strain fracture strain, ε_{fps} .

B. J_{Ic} DETERMINED FROM STRETCH ZONE WIDTH (SZW)

During this research another valuable relationship was determined between the critical J_{Ic} value and the stretch zone width. Upon loading, the sharp fatigue crack undergoes blunting that preceeds the initiation of a ductile crack. This blunting process results in a rather fractureless zone between the fatigue precrack and the ductile fracture; which is called the stretch zone, Figure 20.

Although disagreement exists as to whether the stretch zone height (SZH) or the stretch zone width is the better parameter, Krasowsky and Vainshtok {Ref. 14} have shown satisfactorily that for a stretched zone formed under plane strain with the crack propagation occurring due to microvoid

coalescence with the crack tip, then

$$SZW = \sqrt{2}(SZH) \tag{13}$$

With the knowledge that these two parameters are linearly proportional and that the stretch zone width is much easier to measure, the SZW was selected as the key parameter for further investigation.

Also confusing in this area of study are the conflicting definitions for the stretch zone width {Ref. 14}, {Ref. 24}, and {Ref. 25}. In this research, though, the more common definition was accepted as the horizontal distance between the two aforementioned regions on a horizontally mounted specimen with zero tilt and viewed with a perpendicular incident angle.

Plotting of the calculated SZW for each specimen as listed in Table XI against the DTNSRDC experimental J_{Ic} results provides a well-defined linear relationship for the HY-80 and HY-130 series steels. That the HY-100 specimens do not demonstrate a linear relationship similar to that of the HY-80 and HY-130 steels remains unexplained at this time. Figures 21, 22, and 23 depict this relationship respectively for the HY-80, HY-100, and HY-130 samples.

Several equations defining the SZW in terms of yield strength (σ_y), Young's modulus (E), and fracture toughness (K_{Ic}), have been proposed {Ref. 14}. Recognizing the linear relationship between J_{Ic} and SZW established above invites the acceptance of

$$\frac{K_{Ic}^2}{2E\sigma_y} = a(SZW) \qquad (14)$$

where "a" is a constant. Re-arranging equation (1) into a similar form gives,

$$\frac{K_{Ic}^2}{2E\sigma_y} = \frac{J_{Ic}}{2\sigma_y(1-\nu^2)} \qquad (15)$$

Combining equations, (14) and (15), and solving for J_{Ic} provides,

$$J_{Ic} = 2a(1-\nu^2)\sigma_y(SZW) \qquad (16)$$

Accepting Poisson's ratio as constant for steels, the final equality is,

$$J_{Ic} = A\sigma_y(SZW) \qquad (17)$$

where "A" represents another constant of proportionality. Using the non-prestrained specimen data and solving equation (17) provides a value of "A" equal to 5.64.

Table XI lists all the specimens tested with their calculated SZW, their J_{Ic} values using equation (17), and the DTNSRDC determined J_{Ic} values for comparison. The two J_{Ic} values for each specimen are plotted respectively in Figures 24, 25, and 26 for the three HY-series steels.

Equation (17) has limited applicability since compact tensile specimens must be prepared and tested before the SZW can be measured. However, it still provides for a convenient and alternate method for checking the J_{Ic} fracture toughness parameter with reasonable accuracy.

VI. SUMMARY AND CONCLUSIONS

The following observations have been made:

1. Prestraining of the three HY-series steels to about 5% reduces the fracture toughness approximately one-third from the unstrained value for the HY-100 and HY-130 steels, and slightly less than one-quarter for the HY-80 steel.
2. The fracture surfaces of the prestrained samples show less plasticity than those on the non-prestrained samples, but all samples fractured by microvoid coalescence.
3. Large elongated troughs of low ductility are observed much more frequently on the fracture surfaces of the prestrained samples. The troughs occur in regions rich in alloying elements and increased inclusion content. However, even assuming that these regions can carry no load the reduction in fracture toughness would proportionally be only a few percent, and not the noted 23%-33% above.
4. The stretch zone width was an easily distinguishable physical feature of the fracture that diminished in size with increasing amounts of prestrain. Also, the stretch zone was characteristically narrower around the elongated troughs discussed above, further supporting the concept that these troughs represent regions of reduced plasticity and load carrying capability.

From the above observations the following conclusions were reached:

1. Prestraining results in a reduction in the plane strain fracture strain (ε_{fps}) as calculated from K_{Ic}, COD, and J_{Ic} relationships.

2. The plane strain fracture strain for prestrained samples is approximately equal to the plane strain fracture strain of a non-prestrained sample minus the amount of plastic strain induced by the prestraining.

3. J_{Ic} is shown to be related to the yield strength and ε_{fps} as follows:

$$J_{Ic} \propto \sigma_y (\varepsilon_{fps})^4$$

Thus, although the reduction of the non-prestrained value for ε_{fps} is small, large reductions in J_{Ic} can occur.

4. A method to predict the reduction in J_{Ic} due to prestraining that only requires a knowledge of the J_{Ic} and yield strength of a non-prestrained sample is presented.

5. J_{Ic} is shown to be related to the yield strength and the stretch zone width as follows:

$$J_{Ic} \propto \sigma_y (SZW)$$

Thus, J_{Ic} decreases linearly with decreases in the stretch zone width.

6. The damage mechanism associated with the prestraining is believed to be one in which stress relieving treatments can be used to restore the fracture toughness of the material approximately back to its original, non-prestrained value.

VII. RECOMMENDATIONS

1. Tensile tests, interrupted with stress relieving treatments, should be performed to determine the effect of the stress relieving on the strain hardening rate and the true fracture strain.

2. In conjunction with item #1, further review of the effect of the strain hardening exponent, n, must be conducted to evaluate its influence on the fracture toughness. It is known that the change in "n" is most dramatic at low levels of strain, and it is at these levels where this work's developed equation tends to over-estimate the fracture toughness value.

3. Further investigation should be conducted to validate the use of only the non-strained yield strength, instead of the yield strength at each of the corresponding prestrain levels.

4. Experiments structured along the format outlined by Clausing {Ref. 26} should be conducted to verify the values obtained for the prestrained plane strain fracture strain do indeed equal the non-prestrained plane strain fracture strain minus the amount of plastic strain induced by the prestraining.

5. Further investigation of the HY-100 series steels is required to clarify its failure to follow the obvious trends

established by the HY-80 and HY-130 series steels in regard to their relationships between fracture toughness and plane strain fracture strain and stretch zone width.

6. Additional transmission electron microscopy is required to more fully understand the mechanism of damage due to prestraining.

TABLE I

Composition and Properties

ELEMENT	- - MIL-S-16216 - - HY-80	HY-100	MIL-S-24371 HY-130	- - - - AS TESTED - - - - HY-80	HY-100	HY-130
Carbon	0.18 max	0.20 max	0.12 max	0.16	0.16	0.10
Manganese	0.10-0.40	0.10-0.40	0.60-0.90	0.28	0.27	0.84
Silicon	0.15-0.35	0.15-0.35	0.15-0.35	0.21	0.24	0.25
Nickel	2.00-3.25	2.25-3.50	4.75-5.25	2.09	3.22	4.88
Chromium	1.00-1.80	1.00-1.80	0.40-0.70	1.23	1.58	0.58
Molybdenum	0.20-0.60	0.20-0.60	0.30-0.65	0.23	0.39	0.52
Phosphorus	0.025 max	0.025 max	0.010 max	0.005	0.009	0.007
Sulfur	0.025 max	0.025 max	0.010 max	0.018	0.018	0.005
Titanium	0.02 max	0.02 max	0.02 max	0.002	0.002	0.009
Vanadium	0.03 max	0.03 max	0.05-0.10	0.003	0.003	0.08
Copper	0.25 max	0.25 max	0.25 max	0.16	0.13	0.05
Iron	----------Remainder----------					

MATERIAL	YIELD KSI	TENSILE KSI
HY-180	86.6	100.0
	90.7	103.6
HY-100	111.2	124.4
	108.7	120.9
HY-130	132.8	147.7
	131.2	146.1

HY-80 and HY-100 manufactured by LUKENS STEEL COMPANY
HY-130 manufactured by UNITED STATES STEEL CORPORATION

TABLE II

DTNSRDC J-Integral Results

ALLOY	% PRESTRAIN	DTNSRDC SPECIMEN NUMBER	NEW IN CODE	J_{Ic} (in-lb/in^2)	AVG J_{Ic} (in-lb/in^2)
HY-80 2 INCH PLATE	0	FVM 2	L	862	824
		FVM 3	P	786	
	3	FVM 50	C	596	617
		FVM 51	D	638	
	6.3	FVM 63	E	601	
	7.5	FVM 60	B	505	543
	8.8	FVM 61	X	524	
HY-100 2 INCH PLATE	0	FVO 2	I	981	999
		FVO 4	A	1017	
	3	FVO 32	S	790	735
		FVO 33	T	680	
		FVO 41	Y	737	
	5	FVO 42	U	689	713
		FVO 43	W	713	
HY-130 1½ INCH PLATE	0	FVN 1	J	1402	1249
		FVN 2	K	1096	
	3	FVN 10	H	947	900
		FVN 13	G	852	
		FVN 20	Q	886	
	5	FVN 21	Z	762	845
		FVN 22	R	887	

TABLE III

DTNSRDC Tearing Modulus Instability Results

ALLOY	% PRESTRAIN	DTNSRDC SPECIMEN NUMBER	NEW ID CODE	$\frac{dJ}{da}$	T, TEARING MODULUS	AVG T
	0	FVM 2	L	15835	54.7	51.8
		FVM 3	P	14153	48.9	
HY-80 2 INCH PLATE	3	FVM 50	C	11585	31.2	26.3
		FVM 51	D	7907	21.3	
	6.3	FVM 63	E	5288	14.2	
	7.5	FVM 60	B	4593	12.4	13.5
	8.8	FVM 61	X	5210	14.0	
	0	FVO 2	I	12643	29.3	24.4
		FVO 4	A	8373	19.4	
HY-100 2 INCH PLATE	3	FVO 32	S	8760	20.3	18.2
		FVO 33	T	6975	16.1	
		FVO 41	Y	4607	10.7	
	5	FVO 42	U	6544	15.1	13.3
		FVO 43	W	6123	14.2	
	0	FVN 1	J	15009	20.8	23.8
		FVN 2	K	19295	26.8	
HY-130 1½ INCH PLATE	3	FVN 10	H	16491	22.9	24.1
		FVN 13	G	17239	25.3	
		FVN 20	Q	11626	17.1	
	5	FVN 21	Z	17177	23.9	20.1
		FVN 22	R	13823	19.2	

TABLE IV

Stretch Zone Widths

ALLOY	ID CODE	% PRESTRAIN	SZW(um)
HY-80	L	0	53.1
	P	0	40.1
	C	3	41.9
	D	3	38.0
	E	6.3	28.8
	B	7.5	35.8
	X	8.8	13.3
HY-100	I	0	31.8
	A	0	21.7
	S	3	24.1
	T	3	33.2
	Y	5	16.7
	U	5	37.1
	W	5	34.2
HY-130	J	0	41.0
	K	0	31.8
	H	3	29.7
	G	3	31.2
	Q	5	21.6
	Z	5	21.4
	R	5	22.0

TABLE V

Results of Electron Microprobe Analysis (Relative Counts)

ELEMENT	HY-80		HY-100		HY-130	
	LIGHT	DARK	LIGHT	DARK	LIGHT	DARK
Nickel	4180	4202	6028	6914	8695	8623
	3841	4331	6491	7045	8486	8417
Iron	304736	309158	288106	287582	299765	298926
	308431	307849	288562	289584	300313	299323
Manganese	1752	1656	1224	1584	4312	4458
	1696	1849	1345	1738	4460	4470
Chromium	4964	5276	5625	6320	2040	2028
	5170	5385	5796	6395	2138	2086
Molybdenum	79	111	114	192	139	151
	89	134	162	195	164	181
Vanadium	2	4	32	13	173	192
	11	-14	40	14	177	214
Sulfur	0	8	-6	27	-1	3
	8	40	5	38	-1	14
Silicon	-47	-13	39	140	118	113
	-20	11	54	160	161	183
Carbon	953	1077	1069	974	1088	1064
	1116	1091	1213	991	1213	1223

TABLE VI

DTNSRDC Tensile Test Results

ALLOY/ % PRESTRAIN	ULTIMATE TENSILE STRENGTH (ksi)	YIELD STRENGTH (ksi)	AVERAGE YIELD STRENGTH (ksi)	% ELONGATION	% REDUCTION IN AREA
HY-80/0	104.6	86.9		23	69
	105.3	86.8	86.4	26	70
	102.5	85.4		23	70
/3	107.4	102.8	104.6	22	69
	108.6	106.4		23	70
/5	115.6	115.4	114.9	15	65
	114.6	114.3		13	66
* /6.3			123.3		
* /7.5			130.3		
* /8.8			137.9		
HY-100/0	119.8	101.8		24	73
	116.3	98.0	99.7	25	73
	117.4	99.4		25	73
/3	127.6	119.4	119.4	16	75
	123.5	119.4		20	73
/4	122.6	120.4	120.4	20	68
	122.6	120.4		18	73
* /5			128.6		

*data extrapolated from provided data

TABLE VII

Average Non-Prestrained Constants

ALLOY	J_{Ic} (in-lb/in^2)	σ_y (ksi)	COD (x100 in)	ε_{fps}	B (in)
HY-80	824	86.4	0.530	0.655	0.0518
HY-100	999	99.7	0.557	0.666	0.0509
HY-130	1249	132.0	0.526	0.653	0.0520

TABLE VIII

Calculated ε^{o}_{fps} Using Non-Prestrained Yield Stress.

SPECIMEN/ % PRESTRAIN	J_{Ic} (in-lb/in^2)	σ_y (ksi)	COD (x100 in)	ε_{fps}	+ ε_p	= ε^{o}_{fps}
HY-80						
L/0	862	86.4	0.554	0.666	0.000	0.666
P/0	786	86.4	0.505	0.644	0.000	0.644
C/3	596	86.4	0.383	0.579	0.030	0.609
D/3	638	86.4	0.410	0.596	0.030	0.626
E/6.3	601	86.4	0.386	0.581	0.063	0.644
B/7.5	505	86.4	0.325	0.539	0.075	0.614
X/8.8	524	86.4	0.337	0.548	0.088	0.636
HY-100						
I/0	981	99.7	0.547	0.662	0.000	0.662
A/0	1017	99.7	0.567	0.670	0.000	0.670
S/3	790	99.7	0.440	0.612	0.030	0.642
T/3	660	99.7	0.379	0.577	0.030	0.607
Y/5	757	99.7	0.411	0.596	0.050	0.646
U/5	689	99.7	0.384	0.580	0.050	0.630
W/5	713	99.7	0.397	0.588	0.050	0.638
HY-130						
J/0	1402	132.0	0.590	0.678	0.000	0.678
K/0	1096	132.0	0.461	0.623	0.000	0.623
H/3	947	132.0	0.399	0.589	0.030	0.619
G/3	852	132.0	0.359	0.564	0.030	0.594
Q/5	886	132.0	0.373	0.573	0.050	0.623
Z/5	762	132.0	0.321	0.550	0.050	0.600
R/5	807	132.0	0.373	0.573	0.050	0.623

ε^{o}_{fps} average:

HY-80 = 0.634 +/- 0.020
HY-100 = 0.642 +/- 0.021
HY-130 = 0.622 +/- 0.030

TABLE IX

Calculated ε^{o}_{fps} Using Prestrained Yield Stresses

SPECIMEN % PRESTRAIN	J_{Ic} (in-lb/in^2)	σ_y (ksi)	COD (x100 in)	ε_{fps}	+ ε_p	= ε^{o}_{fps}
HY-80						
L/0	862	86.4	0.554	0.606	0.000	0.606
P/0	786	86.4	0.505	0.644	0.000	0.644
C/3	596	104.6	0.317	0.533	0.030	0.563
D/3	638	104.6	0.339	0.550	0.030	0.580
E/6.3	601	123.3	0.271	0.495	0.063	0.558
B/7.5	505	130.3	0.215	0.438	0.075	0.513
X/8.8	524	137.9	0.211	0.433	0.088	0.521
HY-100						
I/0	981	99.7	0.547	0.662	0.000	0.662
A/0	1017	99.7	0.567	0.670	0.000	0.670
S/3	790	119.4	0.368	0.570	0.030	0.600
T/3	680	119.4	0.316	0.532	0.030	0.562
Y/5	737	128.6	0.318	0.534	0.050	0.584
L/5	689	128.6	0.298	0.518	0.050	0.568
M/5	713	128.6	0.308	0.526	0.050	0.576

ε^{o}_{fps} average:

HY-80 = 0.578 +/- 0.058
HY-100 = 0.603 +/- 0.045

TABLE X

Calculated J_{Ic} Results Using Fracture Strain

SPECIMEN/ % PRESTRAIN	ε^{o}_{fps}	- ε_p	= ε_{fps}	$(\varepsilon_{fps})^4$	J_{Ic} (eq. 4)$_2$ (in-lb/in^2)	J_{Ic} DTNRSDC$_2$ (in-lb/in^2)
HY-80						
L/0	0.655	0.000	0.655	0.184	824	862
P/0	0.655	0.000	0.655	0.184	824	786
C/3	0.655	0.030	0.625	0.153	683	596
D/3	0.655	0.030	0.625	0.153	683	638
E/6.3	0.655	0.063	0.592	0.123	550	601
S/7.5	0.655	0.075	0.580	0.113	506	505
X/8.8	0.655	0.088	0.567	0.103	463	524
HY-100						
I/0	0.666	0.000	0.666	0.197	998	981
A/0	0.666	0.000	0.666	0.197	998	1017
S/3	0.666	0.030	0.636	0.164	830	790
T/3	0.666	0.030	0.636	0.164	830	680
Y/5	0.666	0.050	0.616	0.144	731	737
U/5	0.666	0.050	0.616	0.144	731	689
W/5	0.666	0.050	0.616	0.144	731	713
HY-130						
J/0	0.653	0.000	0.653	0.182	1248	1402
K/0	0.653	0.000	0.653	0.182	1248	1096
H/3	0.653	0.030	0.623	0.151	1034	947
G/3	0.653	0.030	0.623	0.151	1034	852
Q/5	0.653	0.050	0.603	0.132	907	886
Z/5	0.653	0.050	0.603	0.132	907	782
R/5	0.653	0.050	0.603	0.132	907	887

Constants are,

	B (in)	σ_y (ksi)
HY-80 =	0.0518	86.4
HY-100 =	0.0509	99.7
HY-130 =	0.0520	132.0

TABLE XI

Calculated J_{Ic} Results Using Stretch Zone Width .

SPECIMEN/ % PRESTRAIN	σ_y (ksi)	SZW (um)	J_{Ic} (eq. 17)$_2$ (in-lb/in^2)	J_{Ic} DTNSRDC$_2$ (in-lb/in^2)
HY-80				
L/C	86.4	53.1	1019	862
P/0	86.4	50.7	973	786
C/3	86.4	41.9	804	596
D/3	86.4	38.0	729	638
E/6.3	86.4	28.8	553	601
B/7.5	86.4	35.8	687	505
A/8.8	86.4	13.3	255	524
HY-100				
I/C	99.7	31.8	704	981
A/0	99.7	21.7	480	1017
S/3	99.7	24.1	534	790
T/3	99.7	33.2	735	680
Y/5	99.7	16.7	370	737
L/5	99.7	37.1	821	689
W/5	99.7	34.2	757	713
HY-130				
J/C	132.0	41.0	1202	1402
K/0	132.0	31.8	932	1096
H/3	132.0	29.7	871	947
G/3	132.0	31.2	914	852
Z/5	132.0	21.6	633	986
Z/5	132.0	21.4	627	762
K/5	132.0	22.0	645	887

T-L SPECIMEN

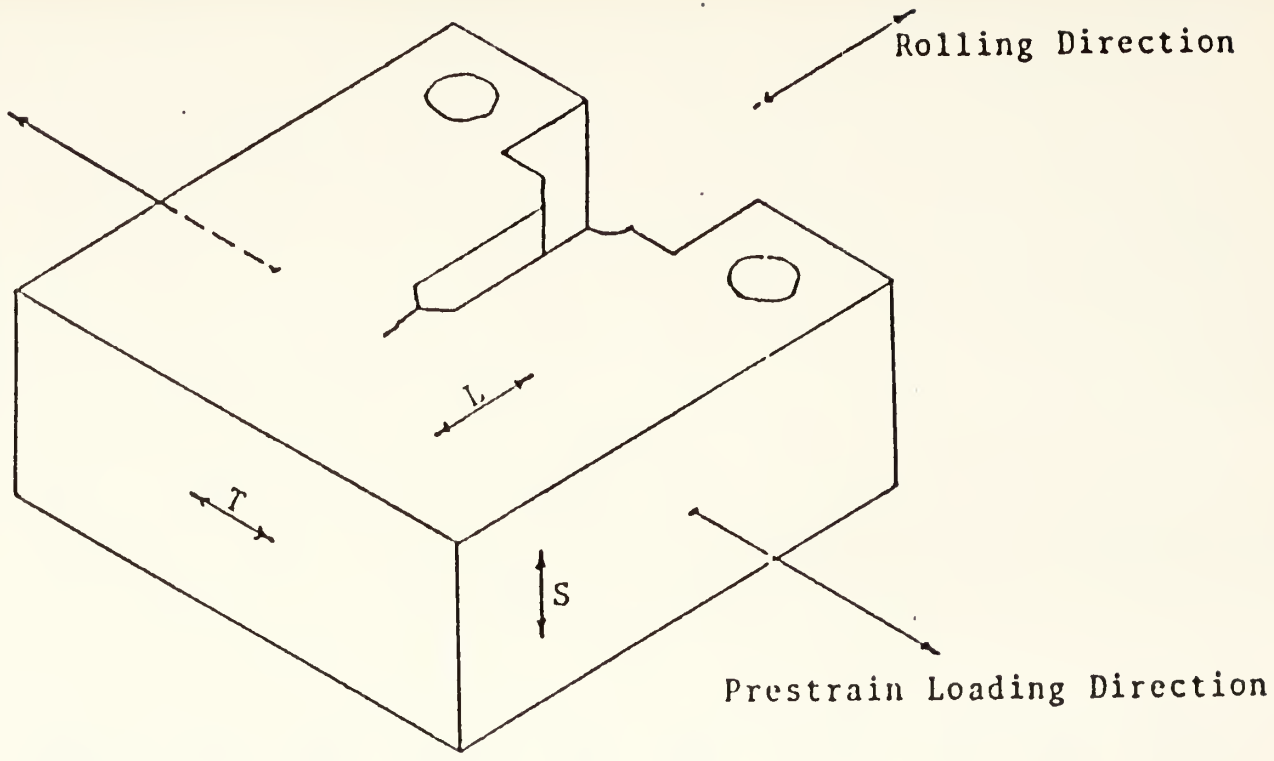

S - Short Transverse
T - Long Transverse
L - Longitudinal Direction

Figure B.1 Test Specimen Orientation

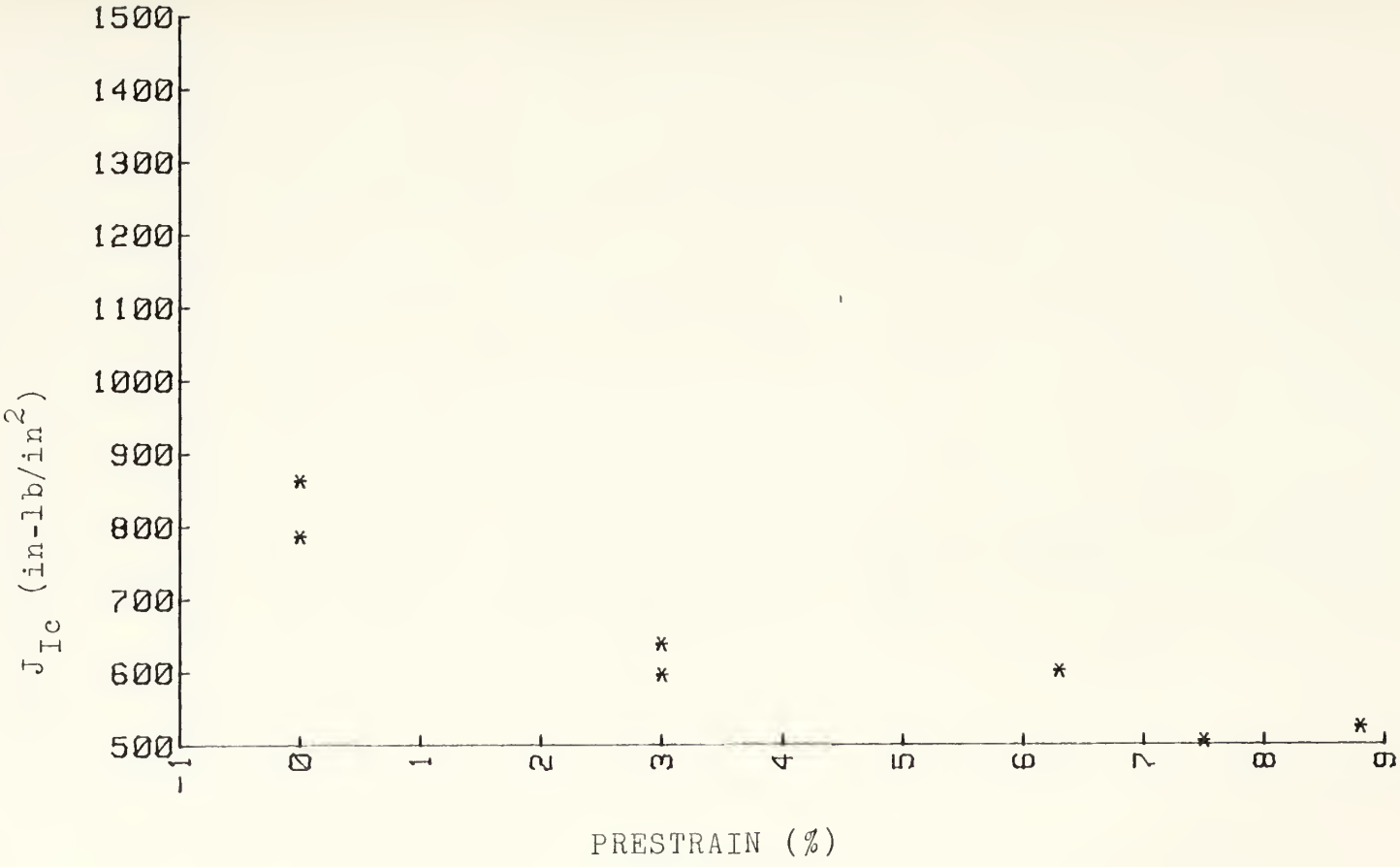

Figure B.2 J_{Ic} versus Prestrain, HY-80

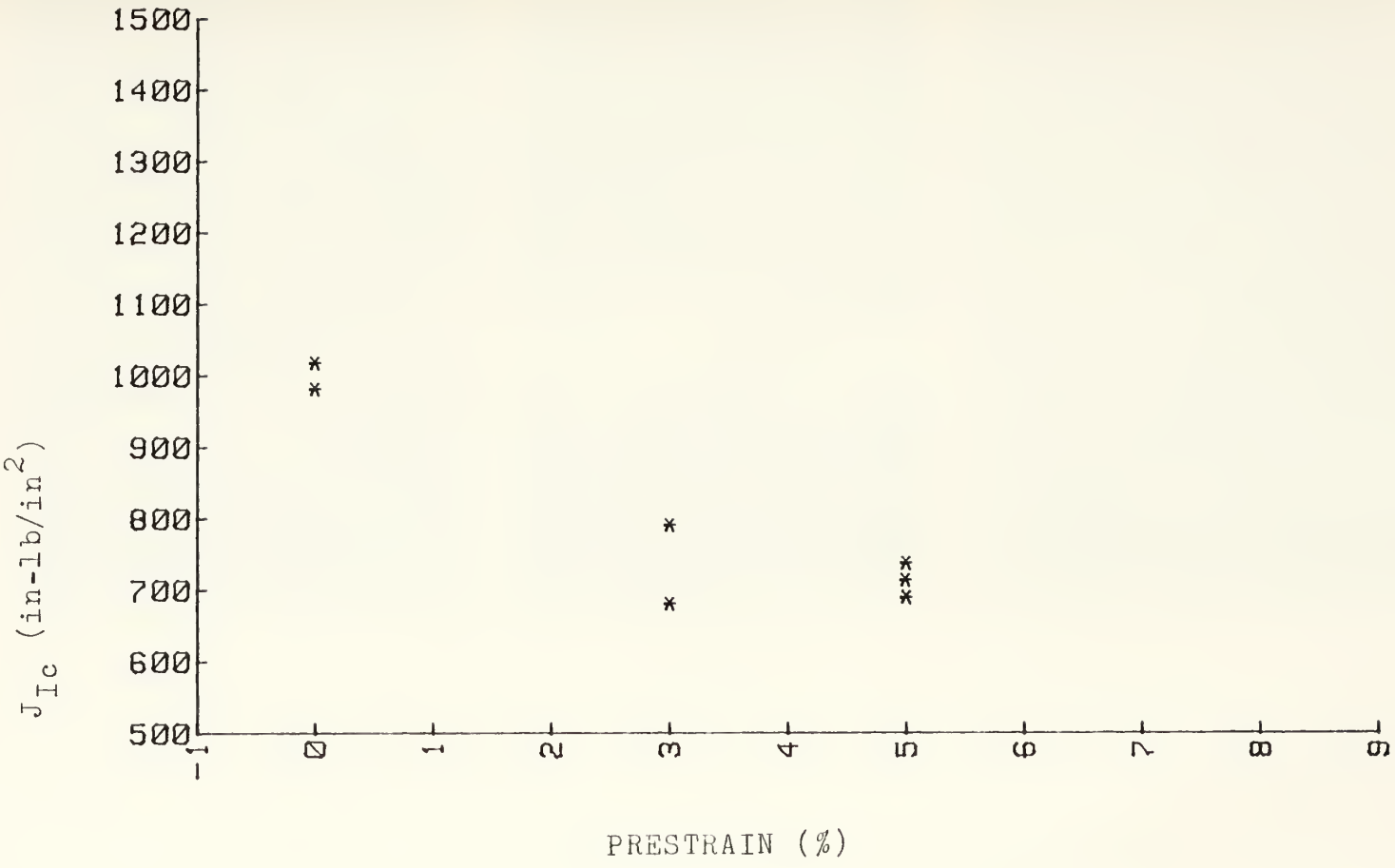

Figure B.3 J_{Ic} versus Prestrain, HY-100

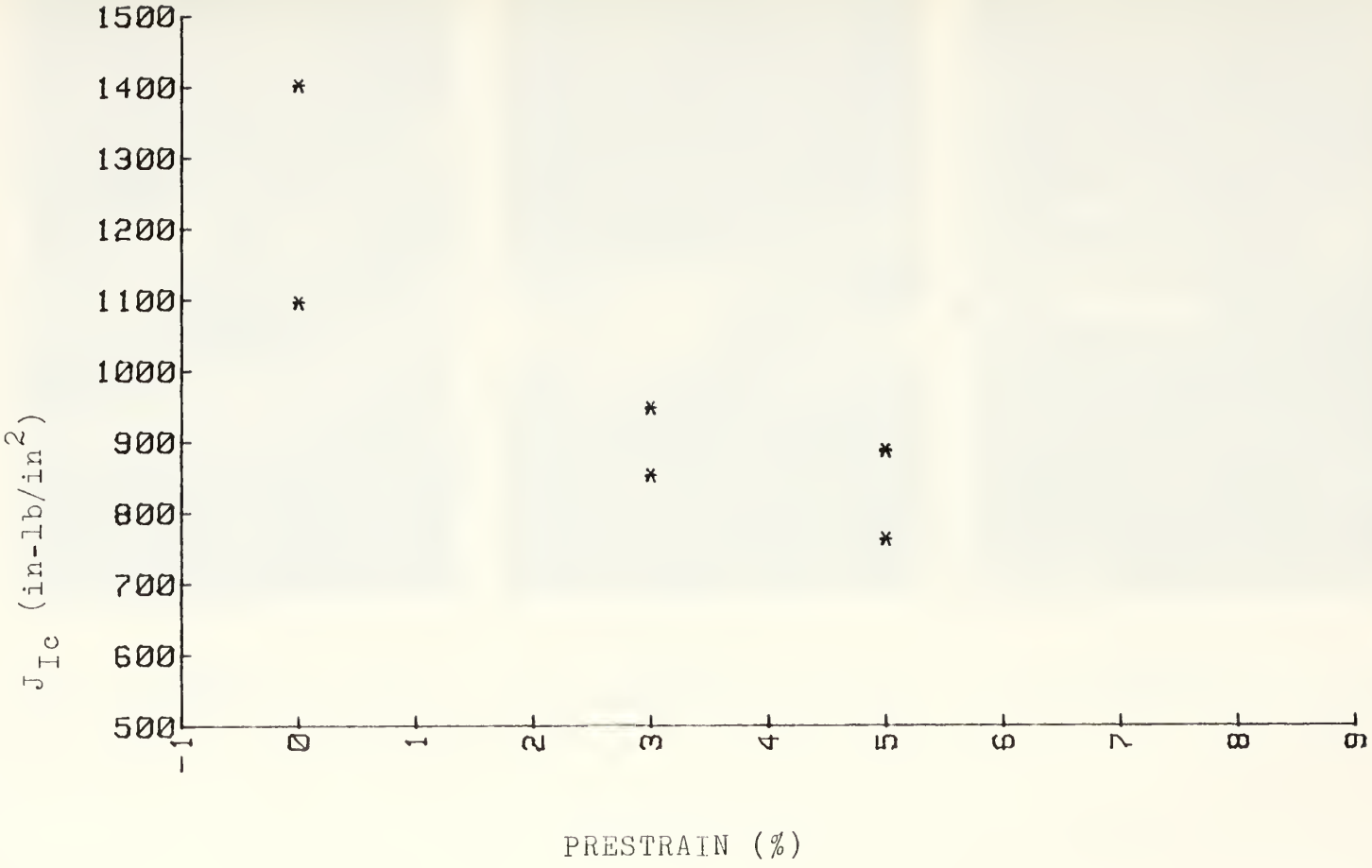

Figure B.4 J_{Ic} versus Prestrain, HY-130

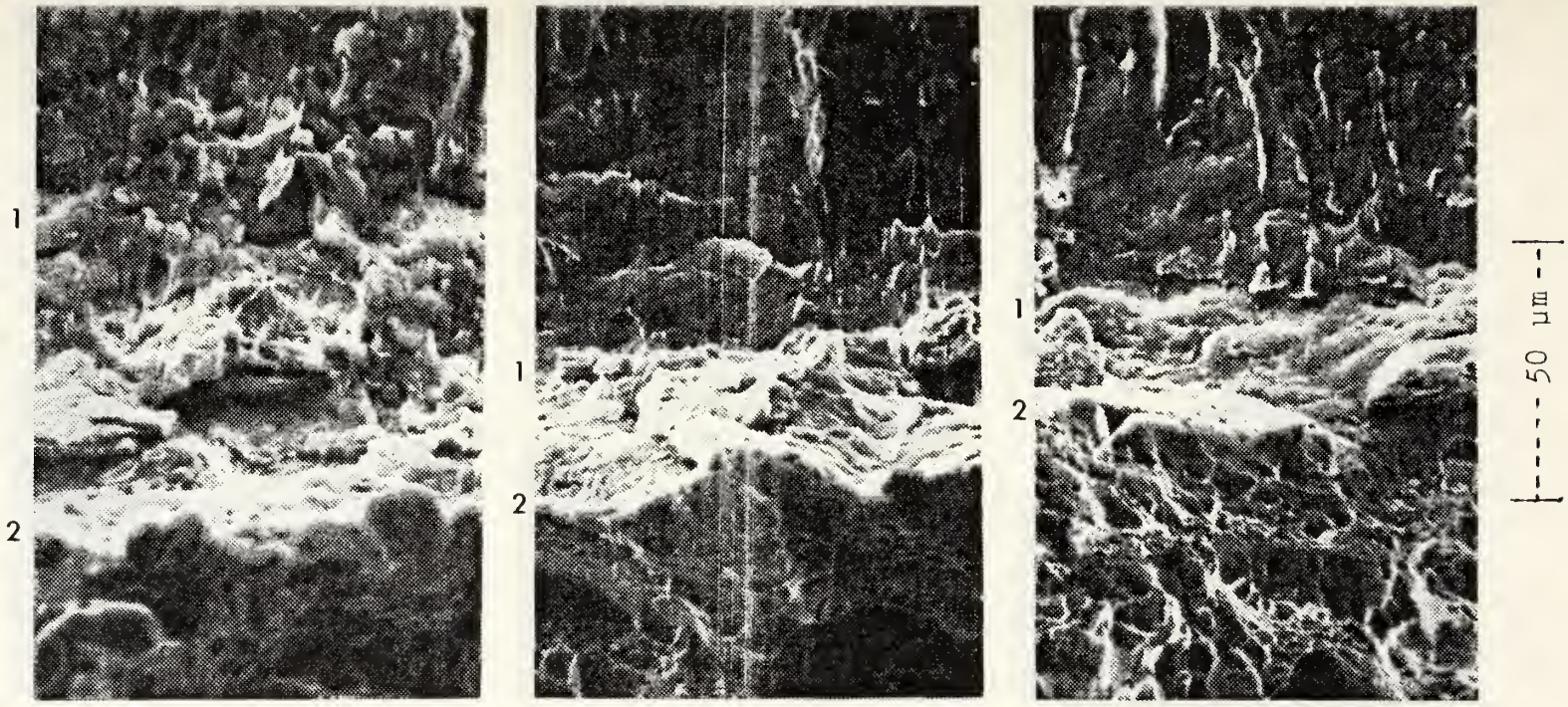

Sample L
0% Prestrain, J_{Ic}=862

Sample C
3% Prestrain, J_{Ic}=597

Sample B
7.5% Prestrain, J_{Ic}=505

Figure B.5 Stretch Zone Width, HY-80 Micrographs

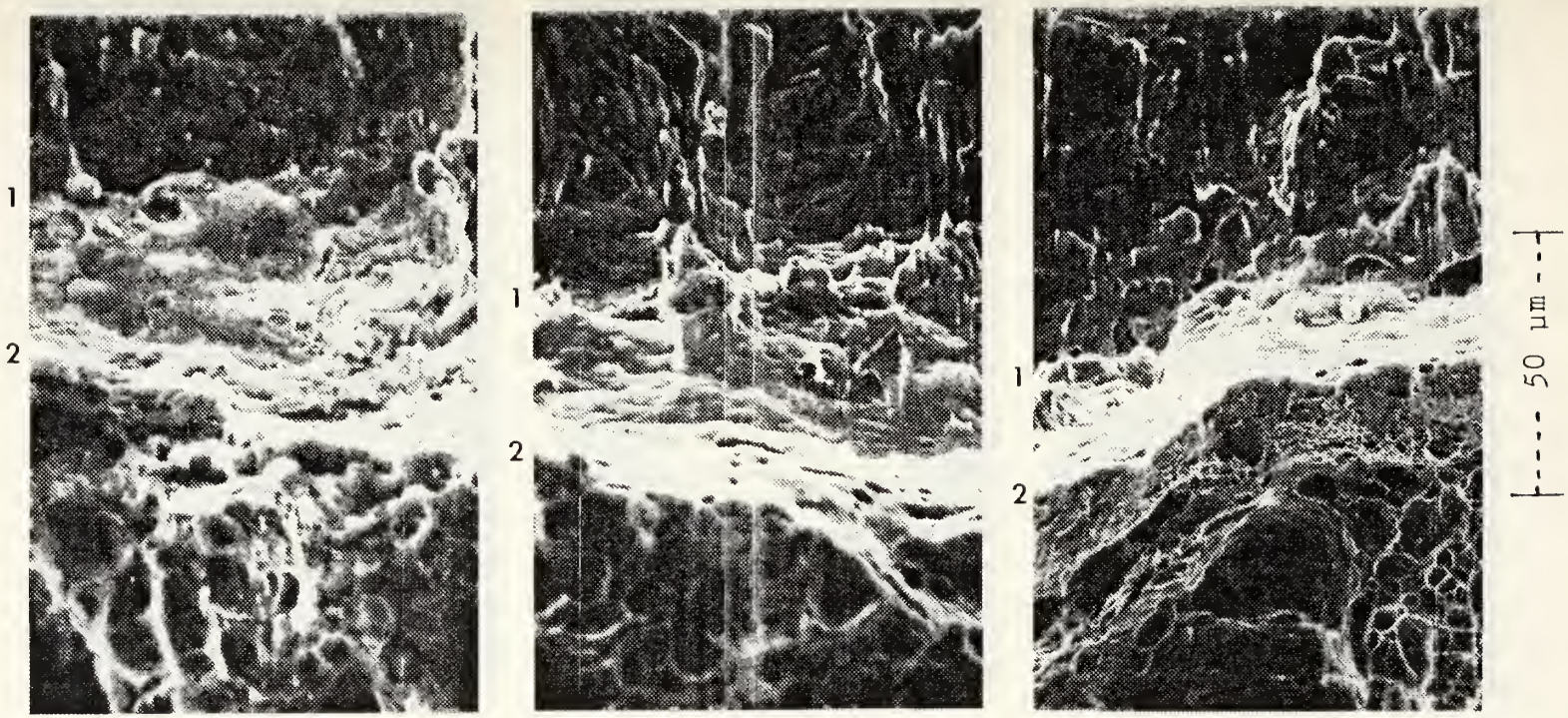

Sample I
0% Prestrain, J_{Ic}=981

Sample S
3% Prestrain, J_{Ic}=790

Sample Y
5% Prestrain, J_{Ic}=737

Figure B.6 Stretch Zone Width, HY-100 Micrographs

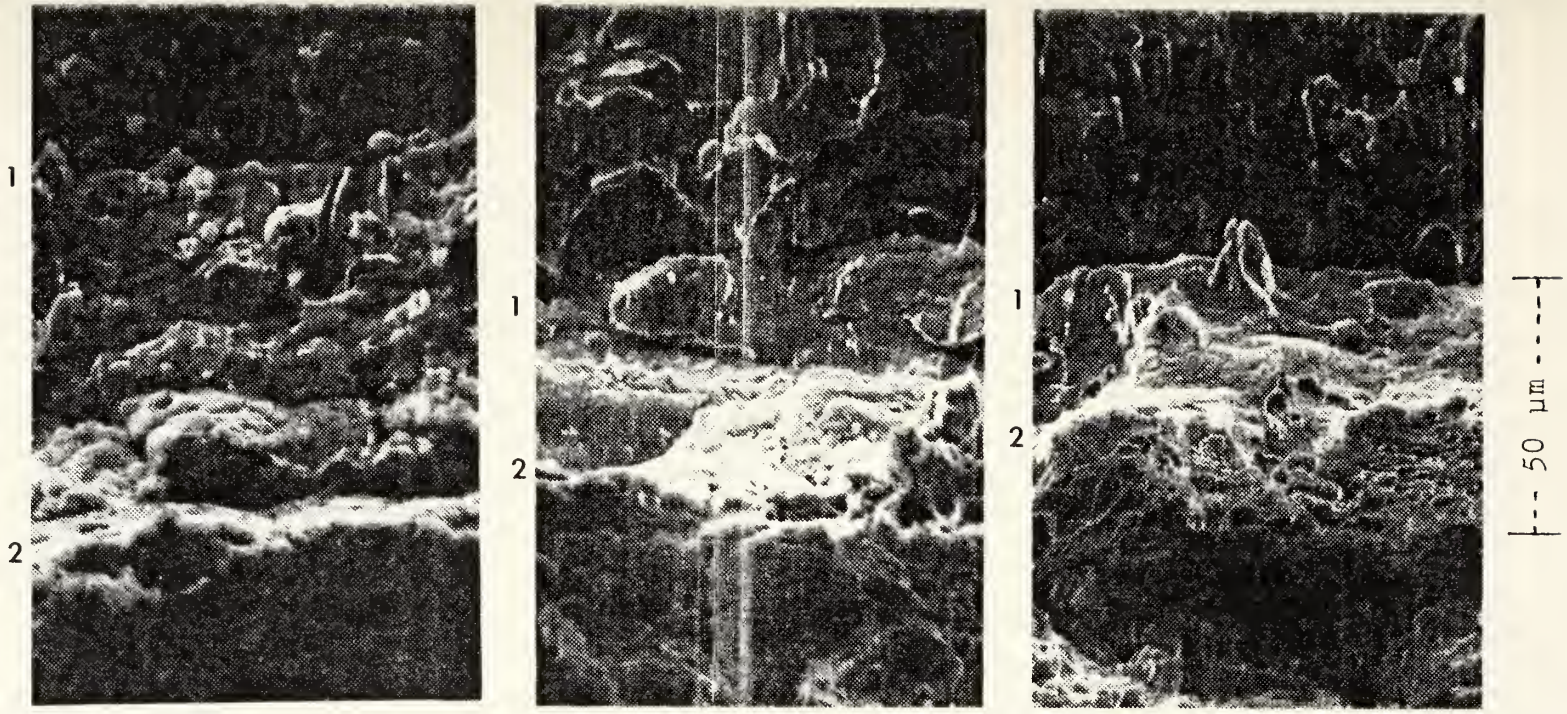

SAMPLE J
0% Prestrain, J_{Ic}=1402

SAMPLE H
3% Prestrain, J_{Ic}=947

SAMPLE Z
5% Prestrain, J_{Ic}=762

Figure B.7 Stretch Zone Width, HY-130 Micrographs

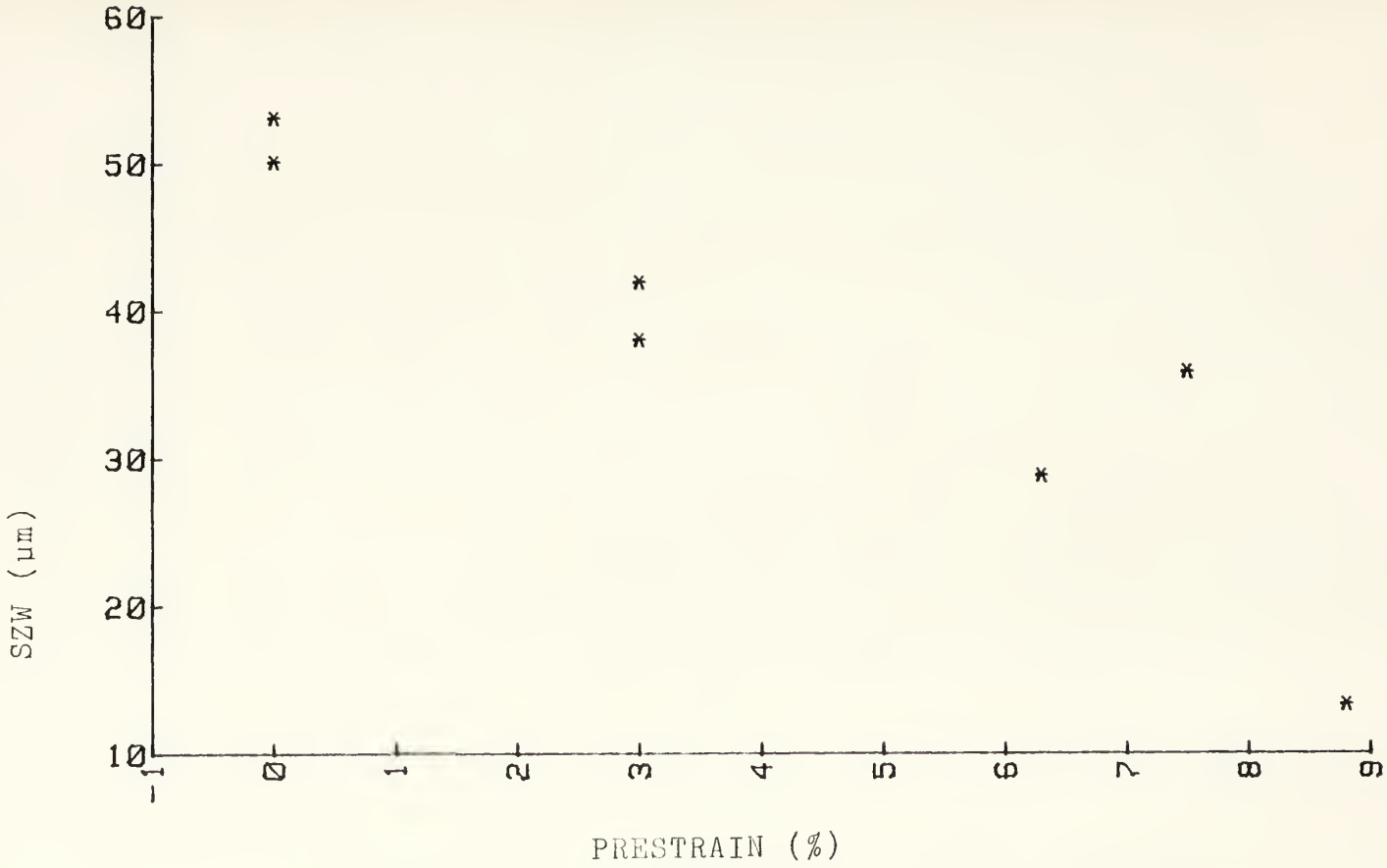

Figure B.8 Stretch Zone Width versus Prestrain, HY-80

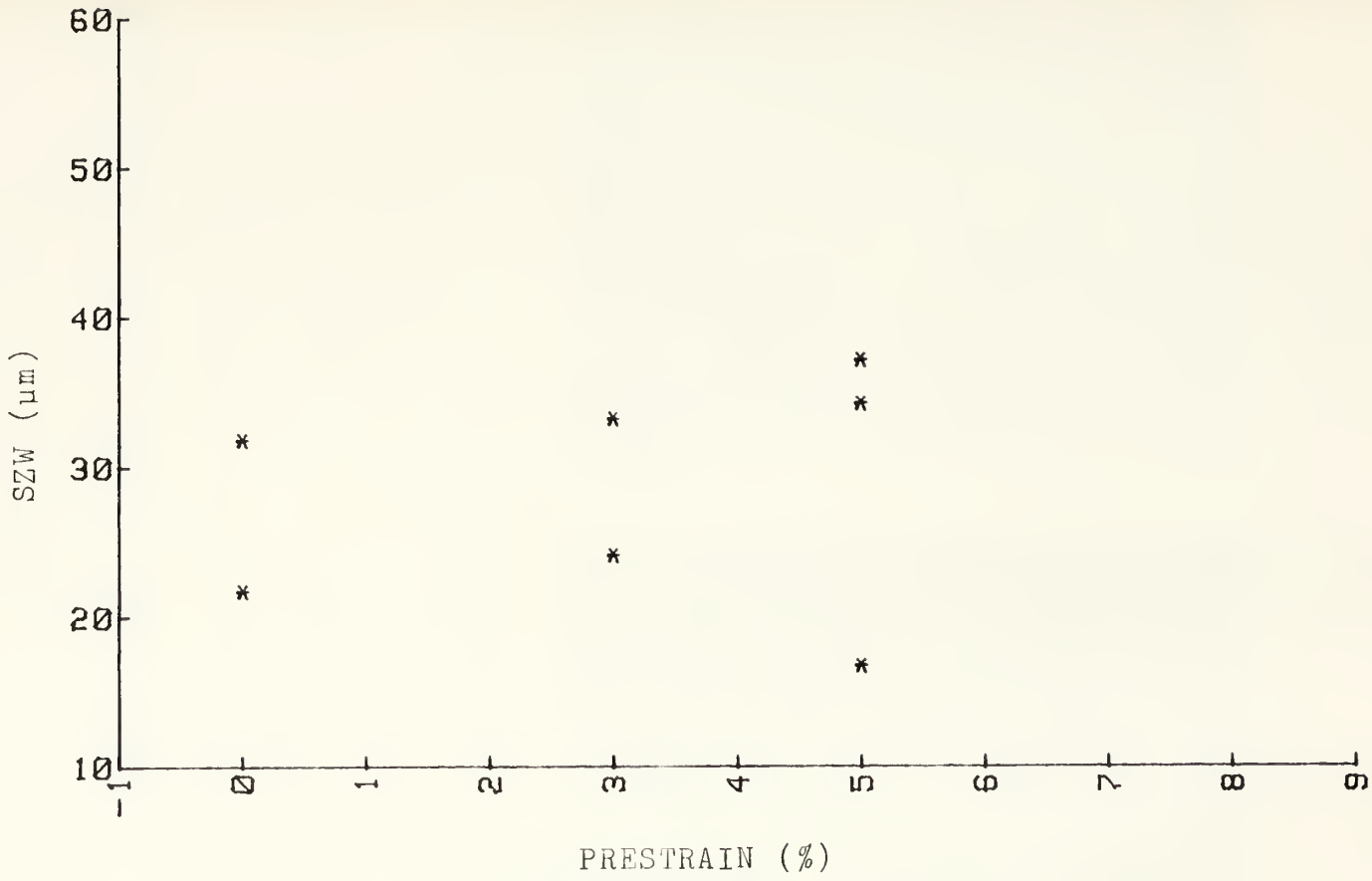

Figure B.9 Stretch Zone Width versus Prestrain, HY-100

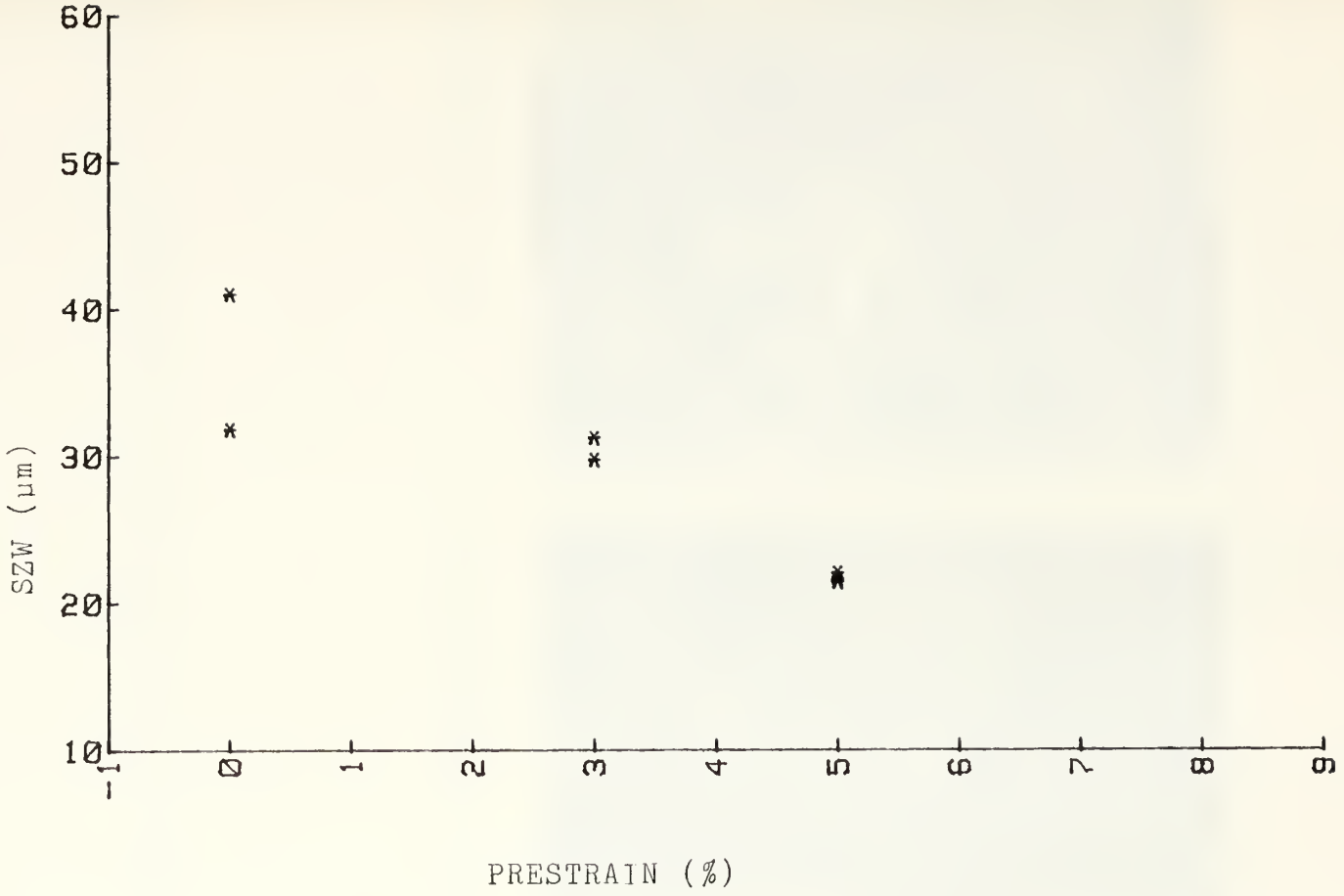

Figure B.10 Stretch Zone Width versus Prestrain, HY-130

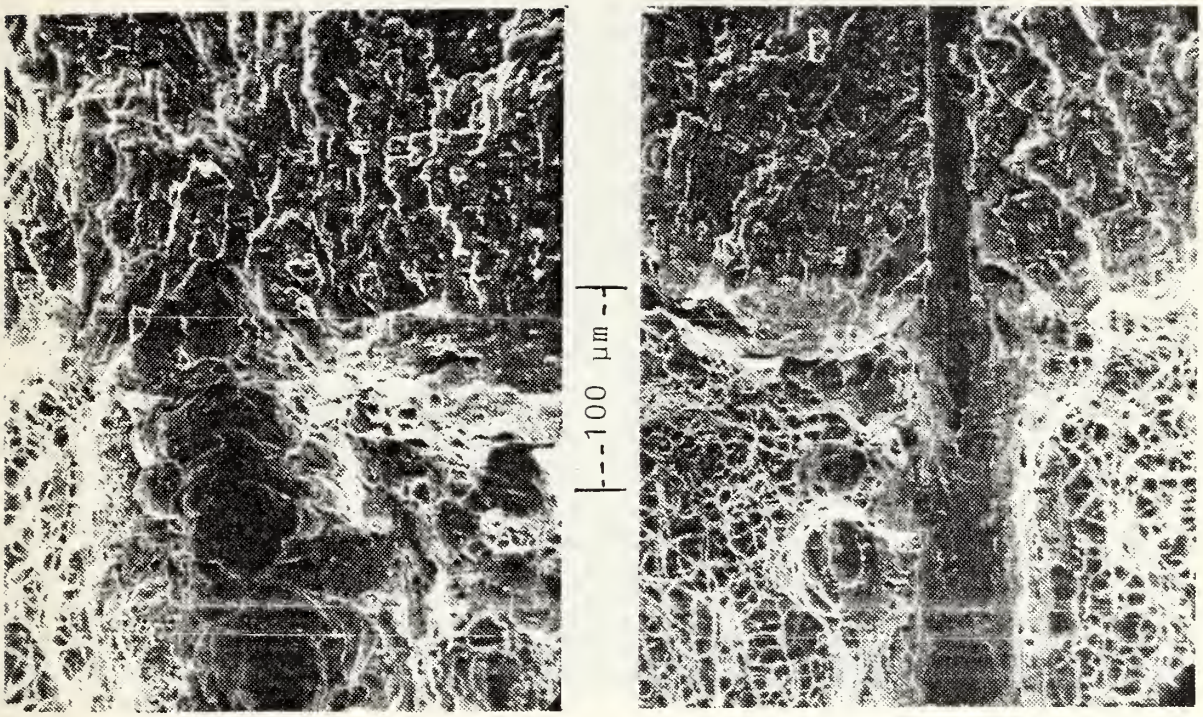

Sample C
3% Prestrain, J_{Ic}=596

Sample X
8.8% Prestrain, J_{Ic}=524

Figure B.11 Elongated Coalesced Microvoid Troughs, HY-80

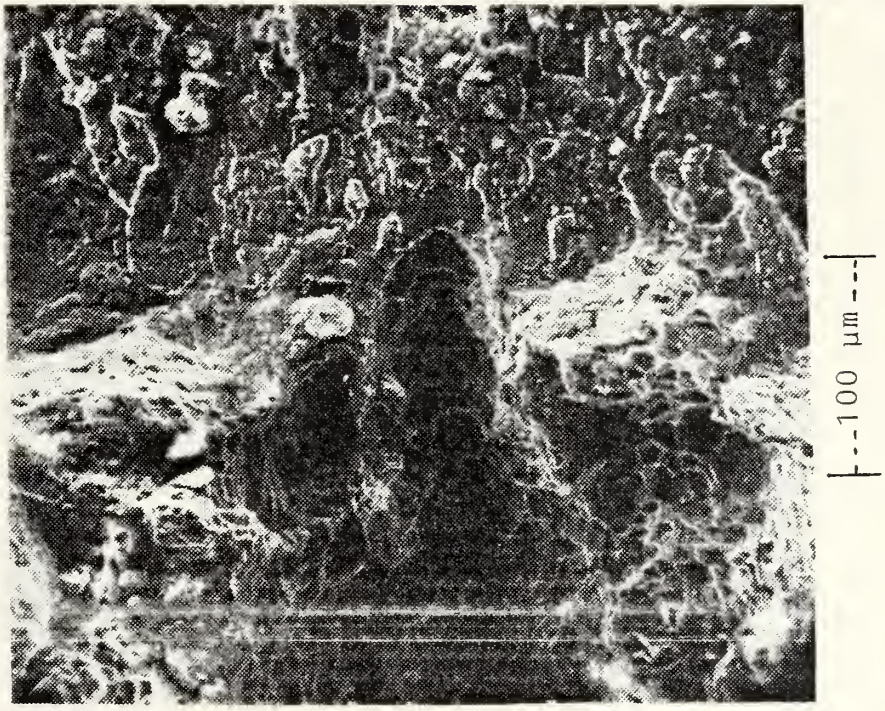

Sample I

0% Prestrain, J_{Ic}=981

Figure B.12 Elongated Coalesced Microvoid Troughs, HY-100

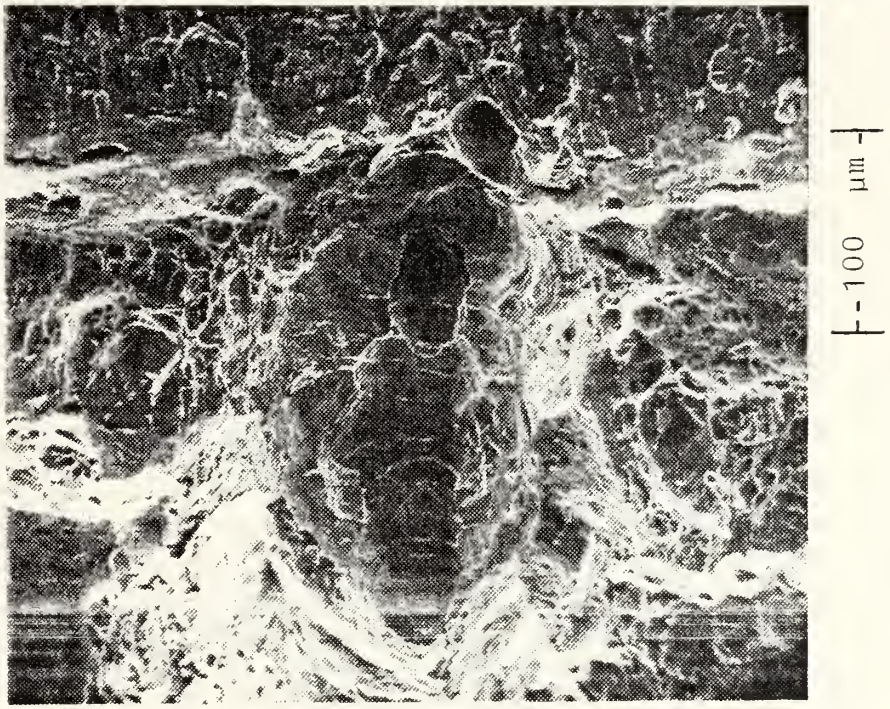

Sample G

3% Prestrain, J_{Ic}=852

Figure B.13 Elongated Coalesced Microvoid Troughs, HY-130

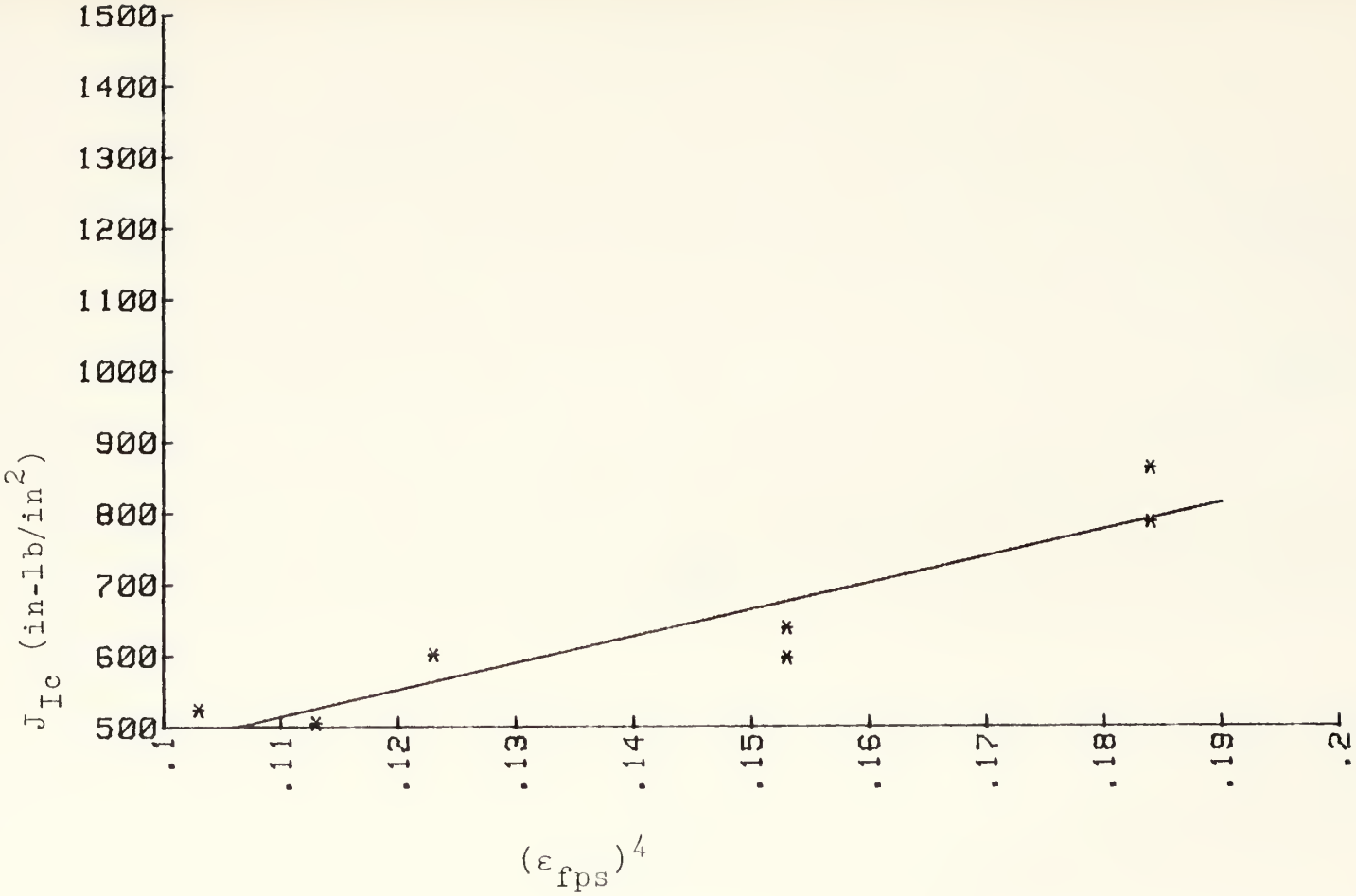

Figure B.14 J_{Ic} versus $(\varepsilon_{fps})^4$, HY-80

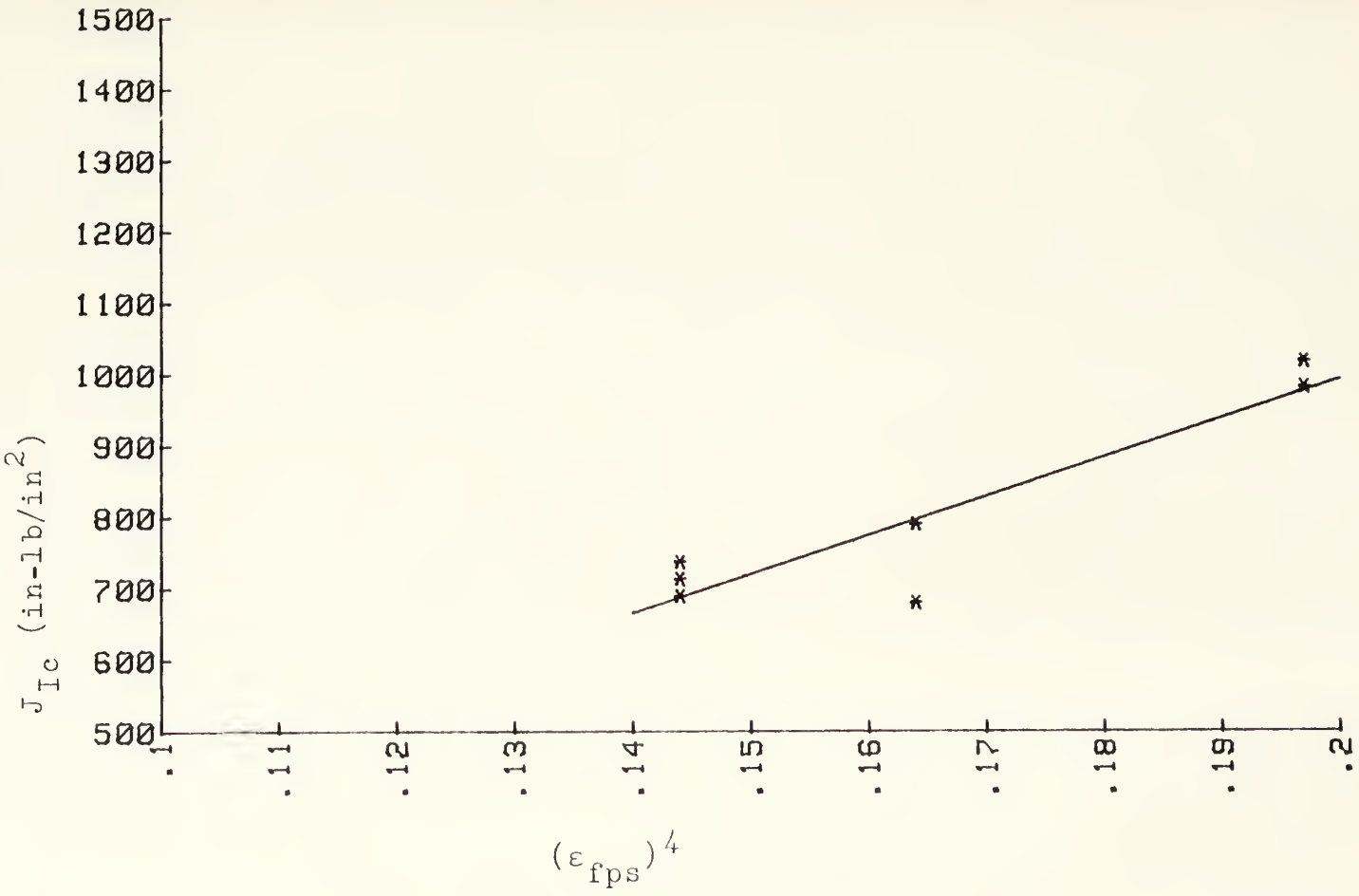

Figure B.15 J_{Ic} versus $(\varepsilon_{fps})^4$, HY-100

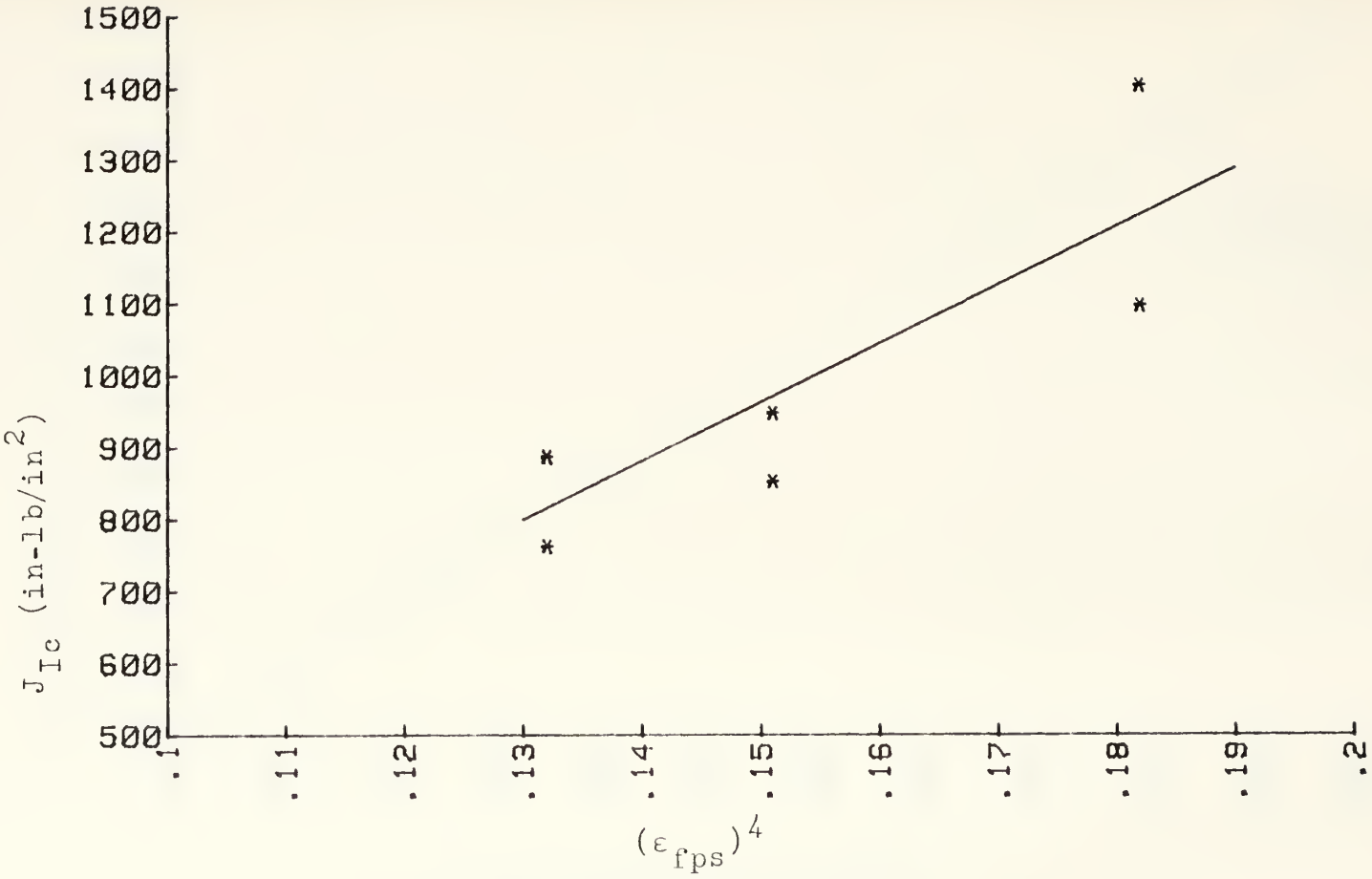

Figure B.16 J_{Ic} versus $(\varepsilon_{fps})^4$, HY-130

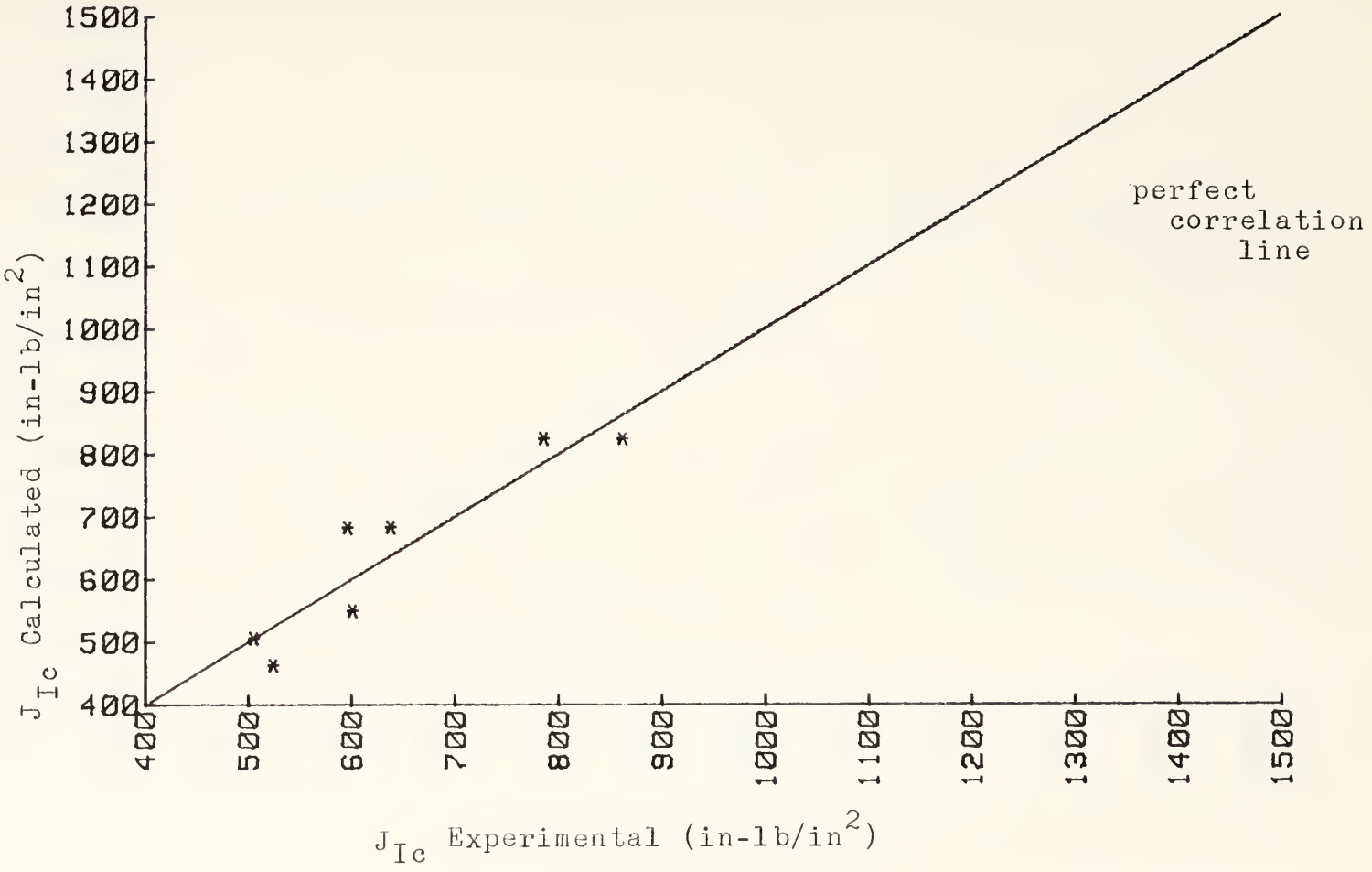

Figure B.17 J_{Ic} Calculated versus J_{Ic} Experimental Using ε_{fps}

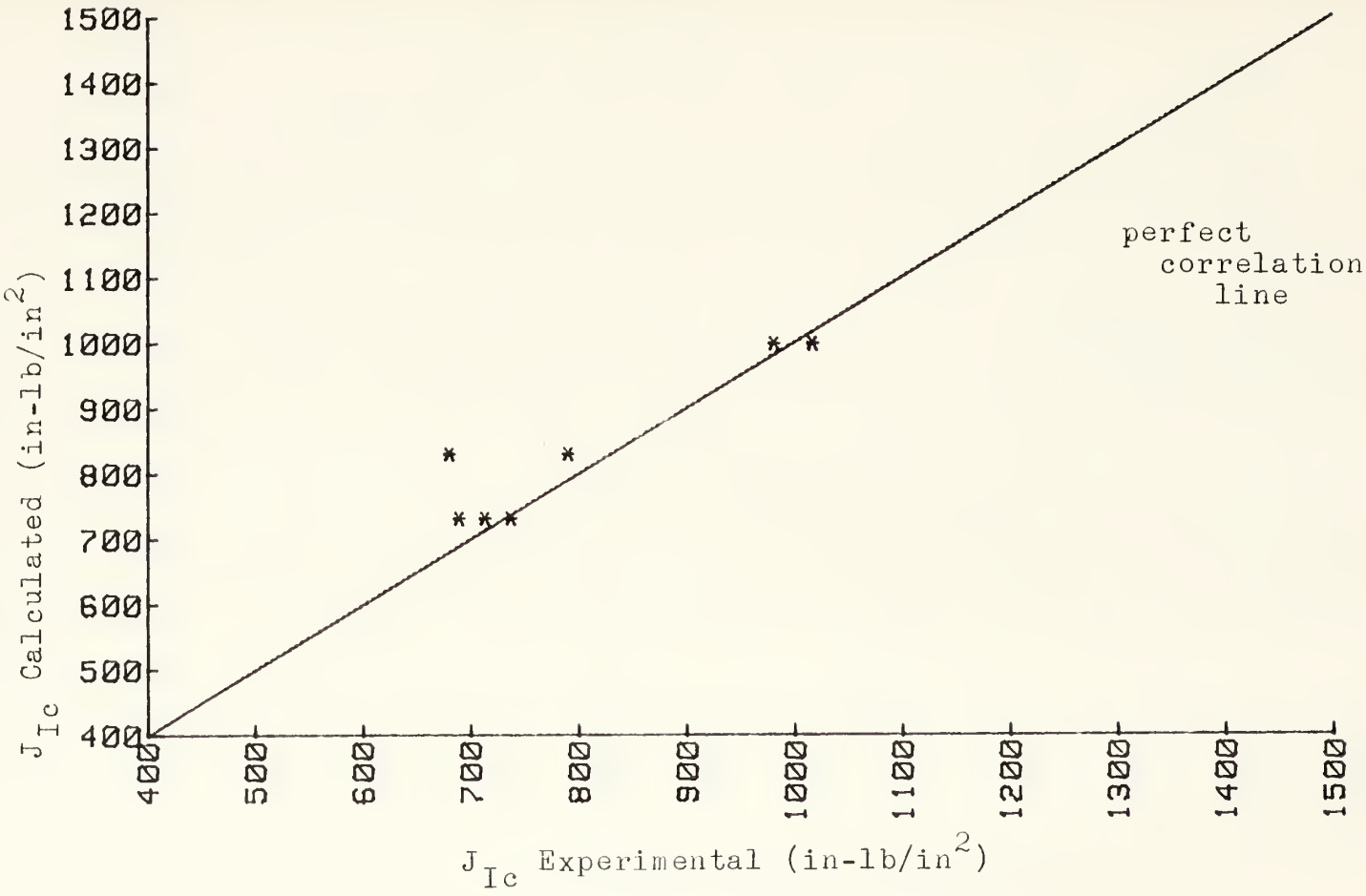

Figure B.18 J_{Ic} Calculated versus J_{Ic} Experimental Using ε_{fps}

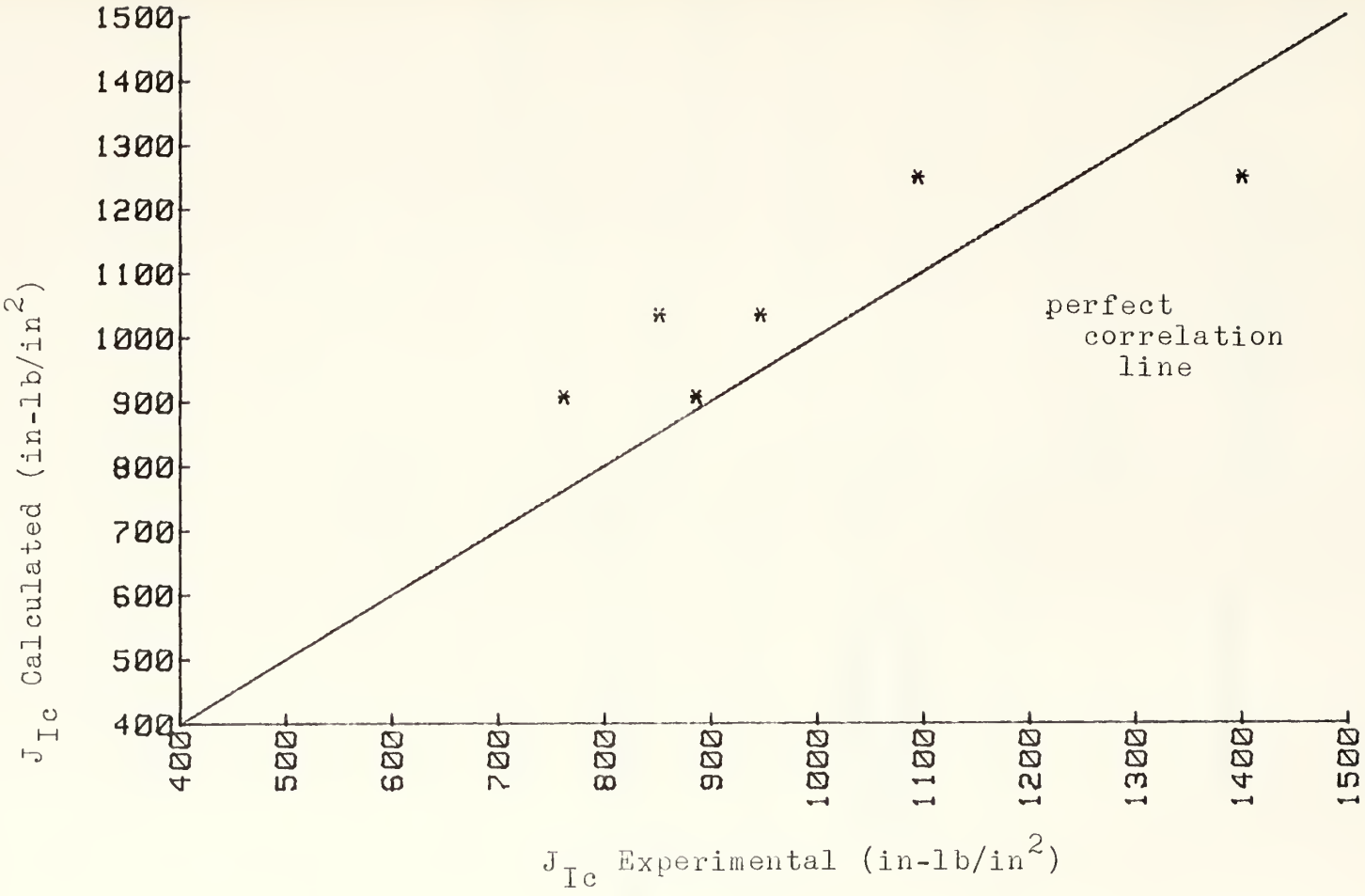

Figure B.19 J_{Ic} Calculated versus J_{Ic} Experimental Using ε_{fps}

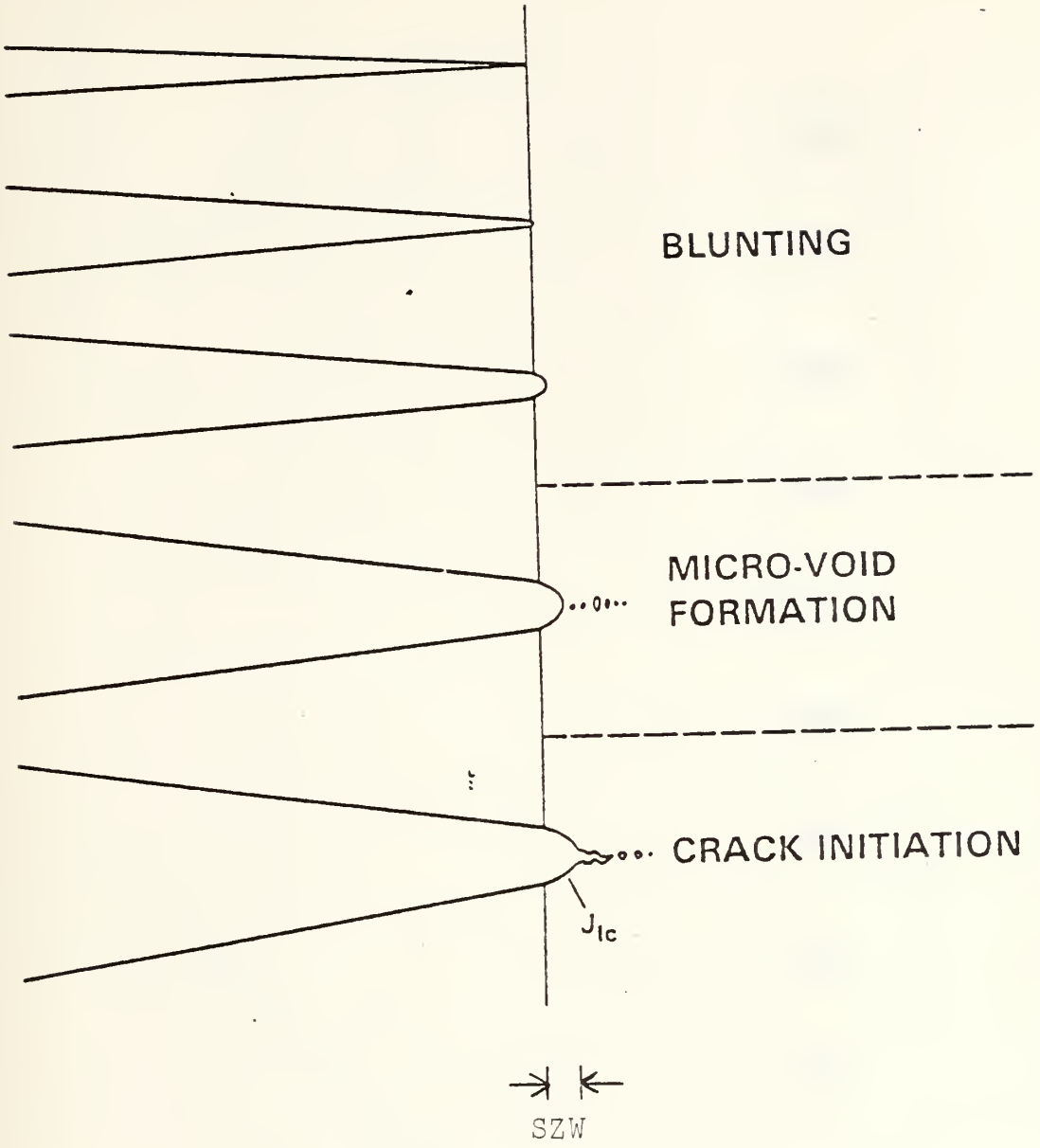

Figure B.20 Stretch Zone Development

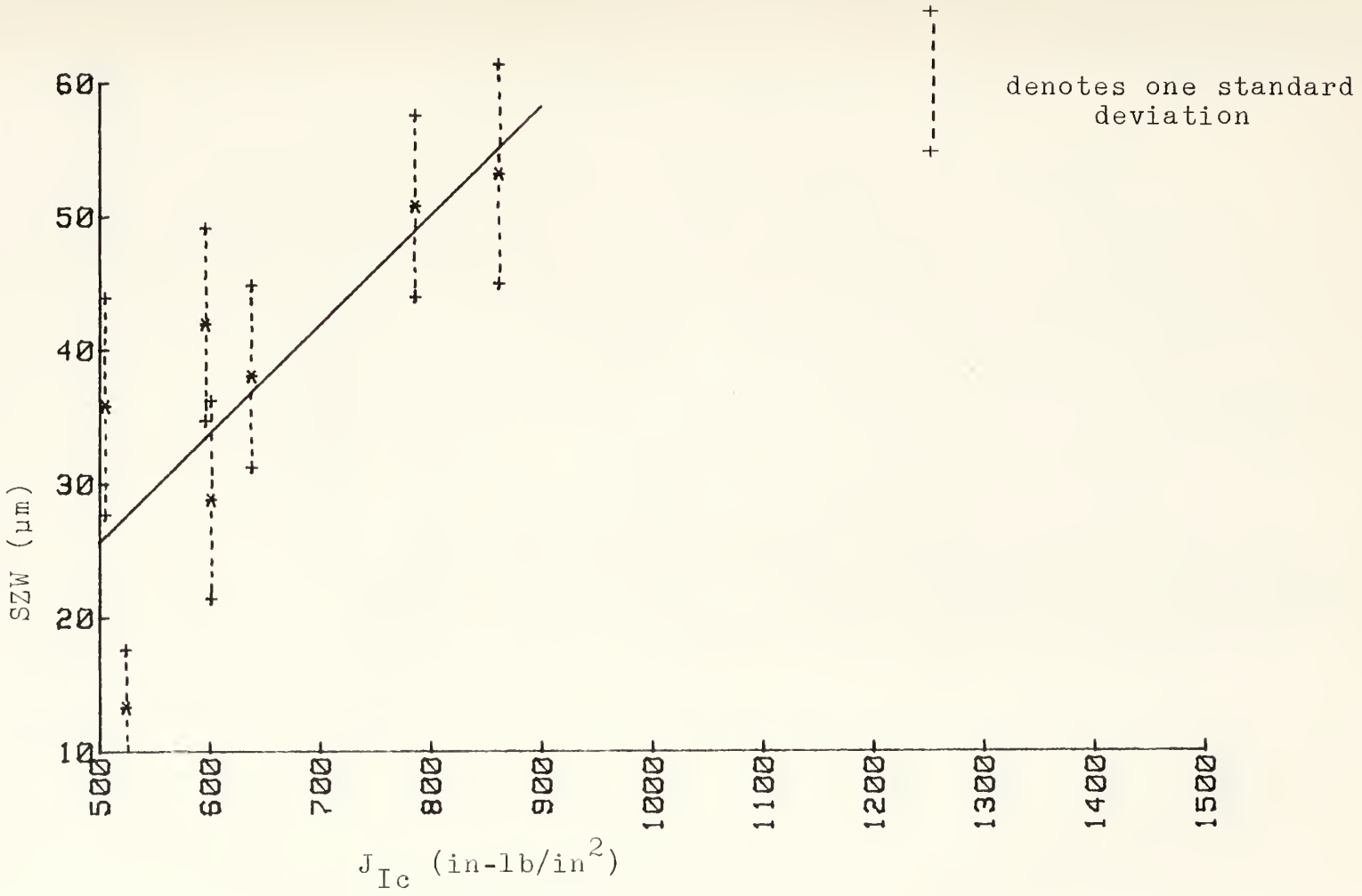

Figure B.21 Stretch Zone Width versus J_{Ic}, HY-80

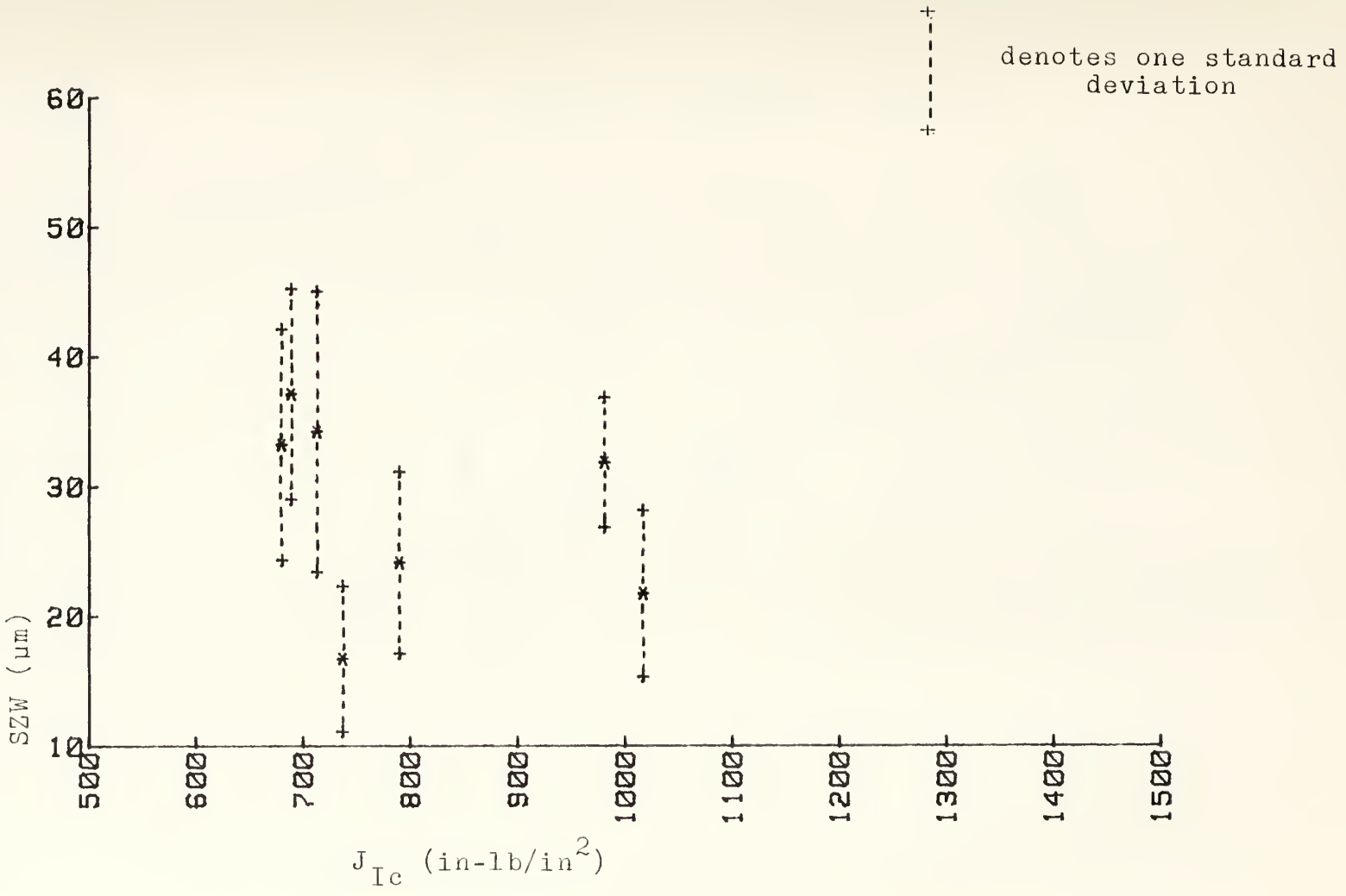

Figure B.22 Stretch Zone Width versus J_{Ic}, HY-100

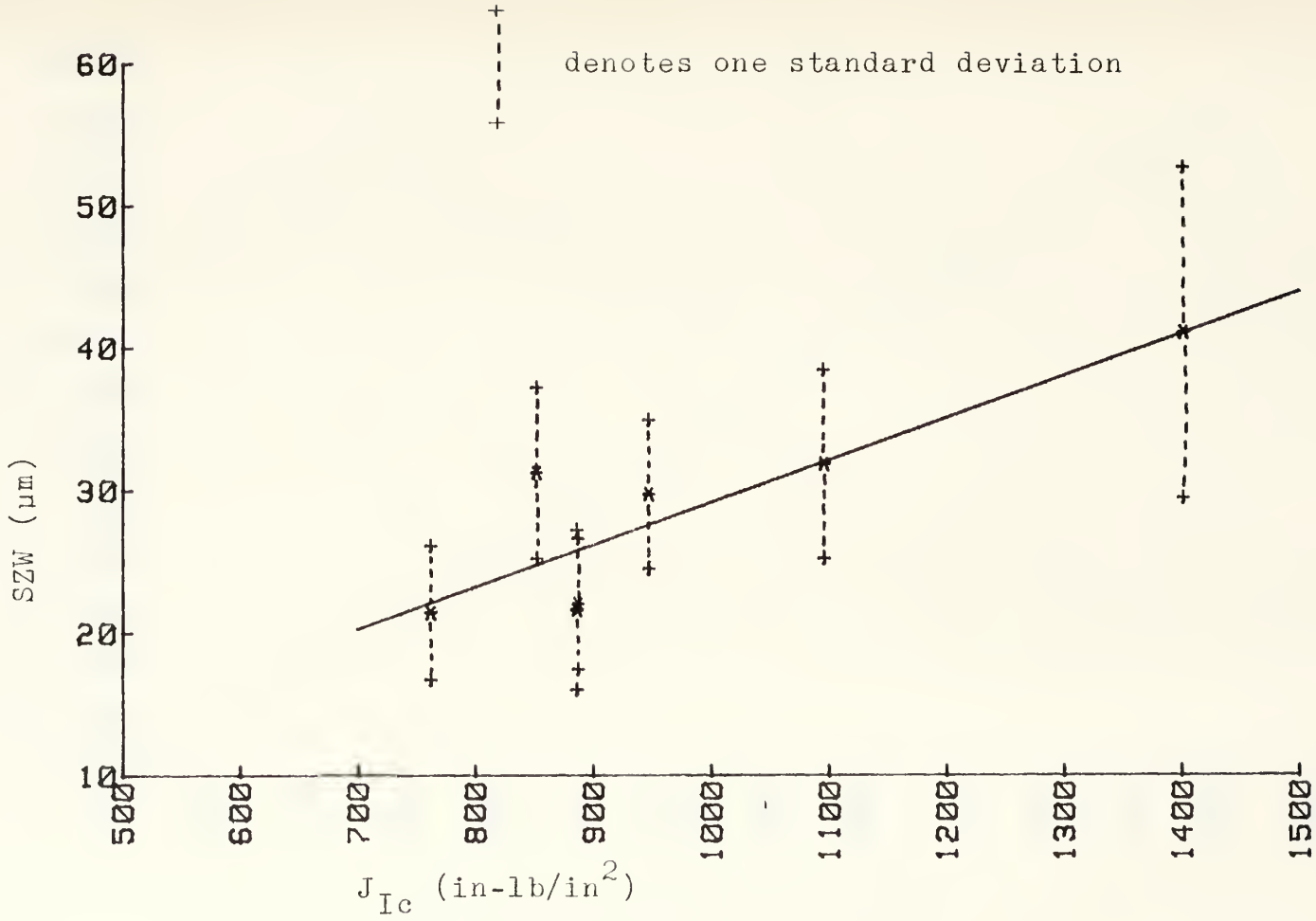

Figure B.23 Stretch Zone Width versus J_{Ic}, HY-130

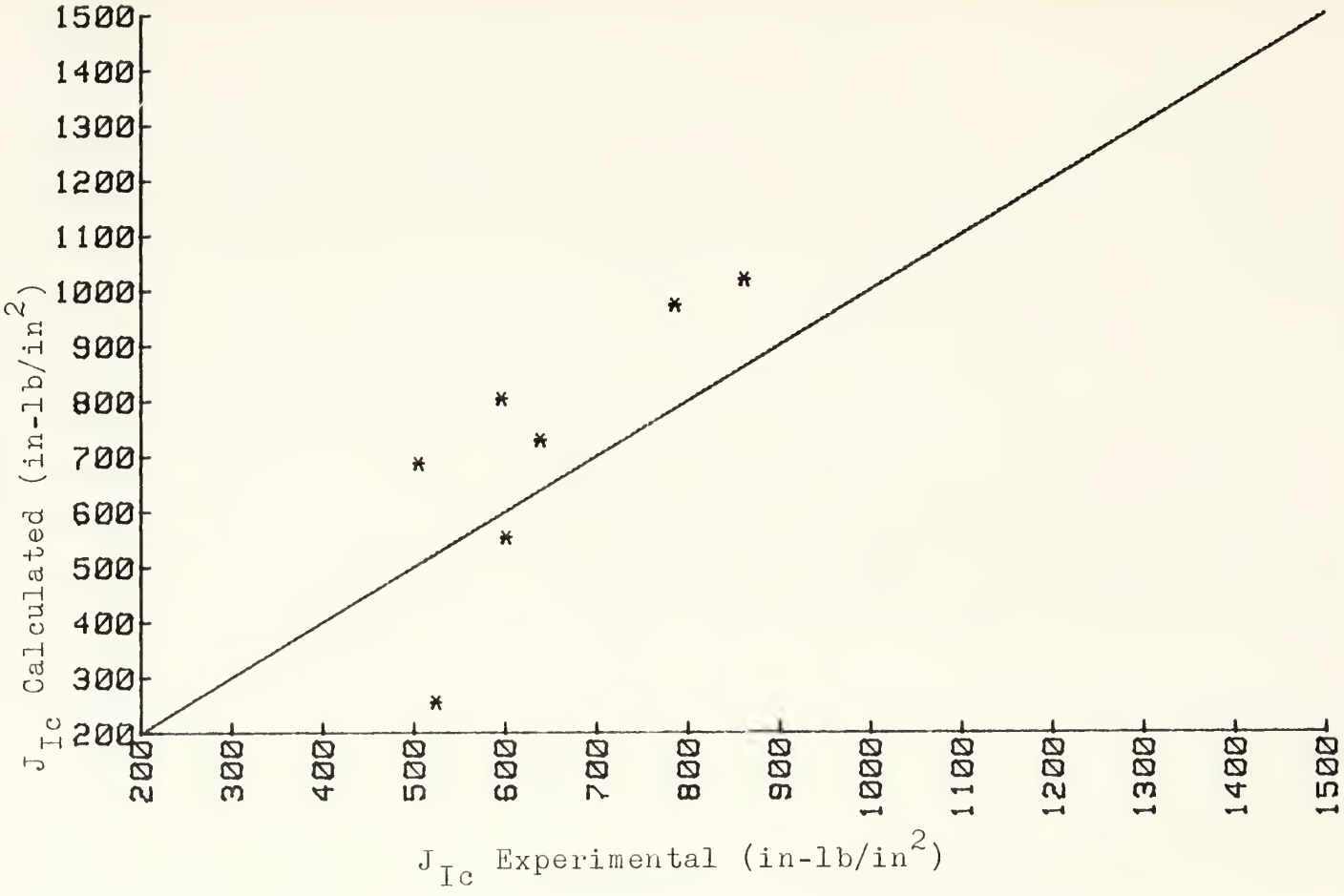

Figure B.24 J_{Ic} Calculated versus J_{Ic} Experimental Using SZW

Figure B.25 J_{Ic} Calculated versus J_{Ic} Experimental Using SZW

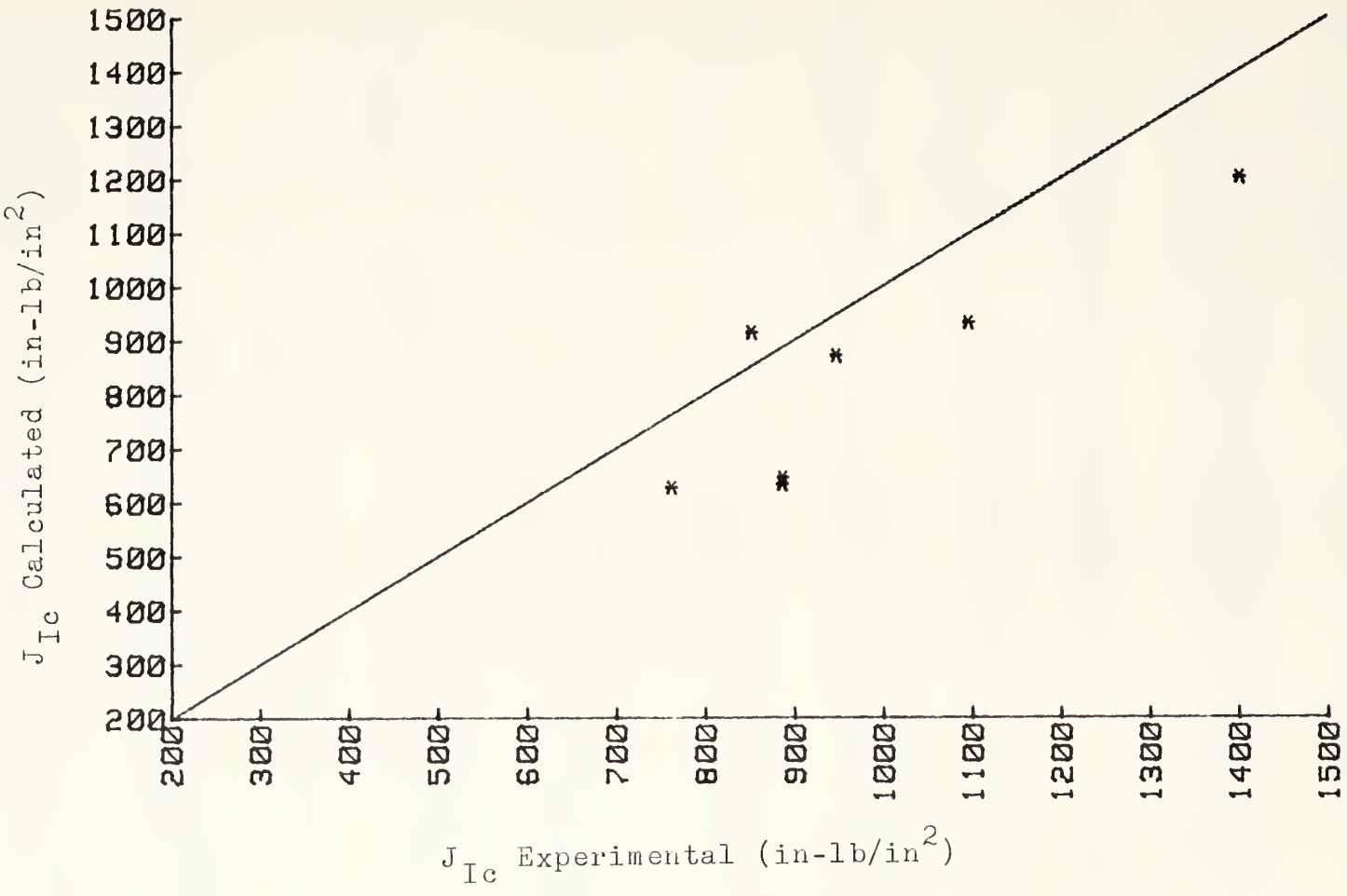

Figure B.26 J_{Ic} Calculated versus J_{Ic} Experimental Using SZW

LIST OF REFERENCES

1. Department of the Navy Military Specification MIL-S-16216H (SHIPS), Military Specification Steel Plate, Alloy, Structural, High Yield Strength (HY-80 and HY-100), 15 March 1972.

2. Department of the Navy Military Specification MIL-S-24371A (SHIPS), Military Specification Steel Plate, Alloy, Structural, High Yield Strength (HY-130), 21 August 1975.

3. Brick, R. M., Pense, A. W., and Gordon, R. B., Structure and Properties of Engineering Materials, pp. 254-277, McGraw-Hill Book Company, 1977.

4. Hertzburg, R. W., Deformation and Fracture Mechanics of Engineering Materials, pp. 292-354, John Wiley and Sons, 1976.

5. The Determination of the Elastic-Plastic Toughness Parameter, J, working document for the ASTM Standards committee, undated.

6. Joyce, J. A., Gudas, J. P., "Computer Interactive J Testing of Navy Alloys," Elastic-Plastic Fracture, ASTM STP 668, pp. 451-468, 1979.

7. Gudas, J. P., Joyce, J. A., and Davis, D. A., "Investigation of Specimen Geometry Modifications to Determine the Conservative J - R Curve Tearing Modulus Using the HY-130 Steel System," Fracture Mechanics, ASTM STP 677, pp. 474-485, 1979.

8. U.S. Nuclear Regulatory Commission, NUREG Report Number 0311, A Treatment of the Subject of Tearing Instability, Paris, P. C., Tada, H., Zahoor, A., and Ernest, H., August 1977.

9. Holman, J. P., Experimental Methods for Engineers, pp. 65-66, McGraw-Hill Book Company, 1978.

10. Structure Probe Technical Report N5392, WDS Analysis of Three Banded Steel Samples (HY-80, HY-100, HY-130), by Normal M. Walter, pp. 1-8, 25 January 1983.

11. David W. Taylor Naval Ship Research and Development Center Report DTNSRDC-81/029, An Experimental Evaluation of Tearing Instability Using the Compact Specimen, by M.G. Vassilaros and J.A. Joyce, pp. 1-20, November 1981.

12. Mullican, J. N., Fracture Toughness Degradation in HY-80 and HY-100 After Prestraining, Engineer's Thesis, Naval Postgraduate School, Monterey, 1983.

13. Begley, J. A., and Landes, J. D., The J-Integral as a Fracture Criterion, Fracture Toughness Proceedings of the 1971 National Symposium on Fracture Mechanics, Part II, ASTM STP 514, American Society for Testing and Materials, 1972.

14. Krasowsky, A. J., and Vainshtok, V. A., "On a relationship between stretched zone parameters and fracture toughness of ductile structural steels," International Journal of Fracture, v. 17, no. 6, pp. 579-592, December 1981.

15. Knott, J. F., Fundamentals of Fracture Mechanics, pp. 167-175, John Wiley and Sons, 1973.

16. Barsom, J. M., and Pellegrino, J. V., "Relationship Between K_{Ic} and Plane-Strain Tensile Ductility and Microscopic Mode of Fracture," Engineering Fracture Mechanics, v. 5, no. 2, pp. 209-221, 1973.

17. Bates, R. C., and Santhanam, A. T., "Relationship Between Notch Tip Strain and Crack-Opening Displacement," Materials Science and Engineering, v. 46, pp. 159-165, 1980.

18. Knott, J.F., "Micromechanisms of fibrous Crack Extension in Engineering Alloys," Metal Science, pp. 327-336, August-September 1980.

19. De Castro, P.M.S.T., Spurrier, J., and Hancock, P., "Comparison of J Testing Techniques and Correlation J-COD using Structural Steel Specimens," International Journal of Fracture, v. 17, no.1, pp. 83-95, February 1981.

20. Fields, B. A. and Miller, K. J., "Fibrous Crack Initiation and Propagation in Prestrained HY-100 Steel," Journal of Mechanical Engineering, pp. 133-143, 1978.

21. Cambridge University Engineering Department Report CUED/C-Mat TR/20, Contract no. AT/2029/0104, The Effect of Prestrain on the Fracture Toughness of HY-100 Steel, by B. A. Fields and K. J. Miller, pp. 1-29, May 1975.

22. Iricibar, R., IeRoy, G., and Embury, J. D., "Relationship of Strain Hardening and Damage in Ductile Fracture," Metal Science, v. 14, pp. 337-343, August-September 1980.

23. Tracey, D. M., "Strain Hardening and Interaction Effects on the Growth of Voids in Ductile Fracture," Engineering Fracture Mechanics, v. 3, pp. 301-315, 1971.

24. Amouzouvi, K. F., and Bassim, M. N., "Determination of Fracture Toughness from Stretch Zone Width Measurement In Predeformed AISI Type 4340 Steel," Materials Science and Engineering, v. 55, pp. 257-262, 1982.

25. Satoh, K., Toyoda, M., and Mutoh, Y., "Effect of Prestrain at Elevated Temperature on the Fracture Behavior of High Strengh Steels," Journal of Engineering Materials and Technology, v. 105, pp. 16-20, January 1983.

26. Clausing, D. P., "Effect of Plastic Strain State on Ductility and Toughness," International Journal of Fracture Mechanics," v. 6, no. 1, pp. 71-85, March 1970.

INITIAL DISTRIBUTION LIST

		No. Copies
1.	Defense Technical Information Center Cameron Station Alexandria, Virginia 22314	2
2.	Library, Code 0142 Naval Postgraduate School Monterey, California 93940	2
3.	Department Chairman, Code 69 Department of Mechanical Engineering Naval Postgraduate School Monterey, California 93940	1
4.	Professor K. D. Challenger, Code 69Ch Department of Mechanical Engineering Naval Postgraduate School Monterey, California 93940	5
5.	Mr. John P. Gudas, Code 2814 David W. Taylor Naval Ship Research and Development Center Annapolis, Maryalnd 21402	1
6.	Mr. Dave R. Anderson, Code 2814 David W. Taylor Naval Ship Research and Development Center Annapolis, Maryland 21402	1
7.	Dr. H. Vanderveldt Ship Systems and Technology NAVSEA Washington, D.C. 20362	1
8.	LCDR Gregory B. Sanford 8220 Lariat Trail NW Bremerton, Washington 98310	3

201650

Thesis
S1637
c.1

Sanford
Degradation of fracture toughness in steels due to prior strain: a predictive model.